Journal of
Food and Packaging
Science, Technique and Technologies

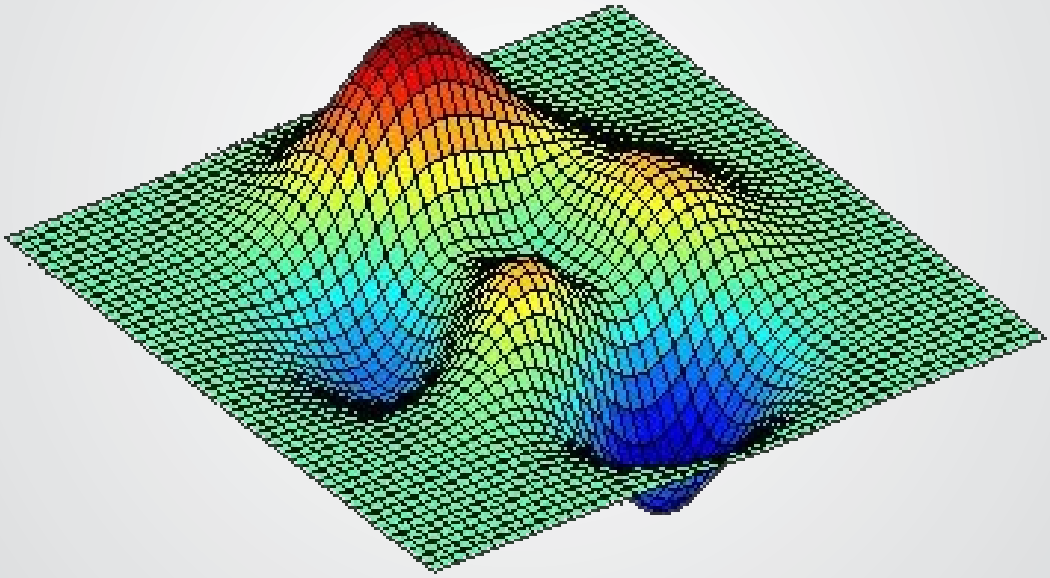

11

ISSN 1314-7773

ISSN 1314-7773

11

Journal of **FOOD** and **PACKAGING** Science, Technique and Technologies

Year V, №11, 2016

National Academy of Packaging - Bulgaria

Web-site: http://mahvp.uft-plovdiv.bg/

Address: 26, Maritza blvd., 4002, Plovdiv, BULGARIA

Phone: +359 32 603 814
+359 32 603 805

E-mail: mahvp@mail.bg
mahvpuht@gmail.com

CONTENT

ABOUT MATERIAL WELDING BY TUBULAR AND DENSE ELECTRODE WIRES

A. Monov[1], I. Zumbilev[2]

[1] Todor Kableshkov University of Transport – Sofia
[2]TU-Sofia, Plovdiv Branch, izumbilev@mail.bg

Abstract. *The aim of the present paper is to make analysis of the geometric parameters of seams, welded by two types of electrode wires – dense and tubular, used in electric arc welding in a gas mixture medium. Mathematical models concerning the geometric parameters have been derived and dependences have been built, reflecting the influence of the technological parameters on the controlled variables.*

Key words: welding, tubular wires, gas mixture, modeling, quality of welded surfaces

I. Introduction.

Electric arc welding in a shielding gas medium is one of the most widely used methods for rehabilitation of worn details. Its advantages are high productivity, technological simplicity, equipment accessibility and possibilities for automation [1, 3, 4].

During the process of their exploitation details in the machines and facilities change the dimensions of their working surfaces due to wear. The rehabilitation of the worn details by welding is a prospective trend in the economy of spare parts, raw materials, and energy. Therefore the rehabilitation of details is widely applied in the developed industrial countries with considerable economic and ecological efficiency [2]. By means of welding the dimensions of the details can be restored, the wear can be reduced, and the deposition of a surface layer with specific properties is also possible. Rehabilitative welding has a high economic efficiency. Complex and expensive detail are thus rehabilitated [6].

One of the prospective methods with wide area of application, combining high productivity with economic efficiency, is welding by means of a tubular wire in a medium of shielding gas mixtures. The process of welding in shielding gas mixtures differs from the other types of welding in that the electric arc burns in a shielding gas jet, and both the weld pool and the drops of electrode metal are protected by the oxygen and the nitrogen in the air and in the gas medium, formed by this jet. One of the main advantages of the method is, that with the help of alloying elements, welded metal with precisely defined properties can be deposited in the cores of the bodies, which is difficult to achieve by welding with a dense wire. Except for alloying elements, gas-forming and slag-forming components are also introduced in the composition of the tubular wire, what ensures protection for the arc and proper performance of the physical and metallurgical processes in the area of welding.

The main parameters, influencing geometry and structure of a weld seam are the current, the voltage and the speed of welding. The quality of the welded layer in case of a wide-layer welding greatly depends on the parameters of the single seams, of which it is composed [1].

The aim of this study is to make a comparative analysis of the geometric parameters and the quality of the welded seams, obtained in flat electric arc welding in a shielding gas medium with use of both a tubular electrode wire Fluxofil 56 and a dense electrode wire LNM 420FM.

II. Methodology of study.

The geometric parameters of the welded layer directly depend on the mode of welding, determined by the current strength I, the voltage U and the speed of welding $\mathbf{V_{WELD}}$. The various combinations between them form a multiplicity of technological modes, leading to a different geometry of the weld seam. Both the shape and the dimensions of the seam are directly related to the productivity in rehabilitating the worn surface and the quality of the welded layer.

A complete factorial experiment of 2^{4-} type was conducted for achieving the goal. Flat samples from steel 20 were welded by two types of electrode wires - Fluxofil 56 and LNM 420FM. The shielding gas mixture was gas corgon, comprising 82% argon and 18% CO_2. Current X_1, voltage X_2, welding speed X_3 and electrode outlet X_4 were used as input factors, and the width B of the welded layer, the height H and the quality K of the welded layer were taken as a target parameter. The range of variation of the controlling factors is given in Table 1.

Table 1. *Interval of variation and factors*

Levels	Main factors			
	X_1 Current [A]	X_2 Voltage [V]	X_3 Welding speed [m/min]	X_4 Electrode outlet [mm]
Basic level (0)	200	22	0,82	13
Range of varying	50	4	0,54	3
Lower level (-1)	150	18	0,28	10
Upper level (+1)	250	26	1,36	16

Each of the geometric parameters of the weld seam (strengthening and width), as well as the quality in welding is described by a law of functioning in compliance, by which the particular parameter reacts to the action of the factors, given in Table 1.

The following equipment was used for conducting the experiments: source of current IZA – G 315; device for feeding the bodies UT-5; automat (tractor) for welding Kometa 2; gas burner RM 36M RZ2 - Imax- 360A (CO2); 320A (Ar+CO_2). The welding was realized with flat test samples, made of steel 20 with dimensions: width 250 mm, length 500 mm, and thickness 20 mm.

In order to achieve higher surface hardness of the welded layer at a minimum area of thermal influence, the following components were chosen: tubular wire Fluxofil 56 – 1,4mm (produced by OERLIKON) DIN 8555, having the following chemical composition in weight percentage - C-0,35 , Mn-1,5 , Si-0,53 , S-0,007 , P-0,012 , Cr-5,2 , Mo-0,64; dense wire LNM 420FM (produced by LINKOLN), with the following chemical composition in weight percentage - C-0,45 , Mn-0,4 , Si-3 , Cr-9,5.

Each of the parameters of quality is controllable by measurement, by assessing it quantitatively in its own limited range of change. The adequacy of the models is defined by the coefficient of multiple correlation and confirmed by the calculated value of the F-criterion of Fisher, which needs to be higher than the tabular value.

III. Results and discussion

A standard methodology was used [5], and for the studied parameters of quality these non-linear dependences were obtained:

For the tubular electrode wire FLUXOFIL 56:

$$B = 6{,}405 + X_1 + 1{,}196X_2 - 1{,}757X_3 - 0{,}076X_4 + 0{,}197X_1^2 + 0{,}24X_1X_2 - 0{,}493X_1X_3 + 0{,}0416X_1X_4 + 0{,}0588X_2^2 - 0{,}268X_2X_3 \quad \text{.....} \quad (1)$$

$$H = 1{,}643 + 0{,}242X_1 - 0{,}212X_2 - 0{,}69X_3 - 0{,}003X_4 - 0{,}017X_1^2 + 0{,}24X_1X_2 - 0{,}096X_1X_3 + 0{,}034X_1X_4 + 0{,}232X_2^2 - 0{,}252X_2X_3 + 0{,}232X_3^2 - 0{,}053X_3X_4 - 0{,}078X_4^2 \quad \text{…} \quad (2)$$

$$K = 2{,}536 + 0{,}148X1 + 0{,}3X_2 - 0{,}648X_3 + 0{,}086X_4 - 0{,}876X_1^2 + 0{,}255X_1X_2 + 0{,}215X_1X_3 + 0{,}091X_1X_4 + 0{,}249X_2^2 - 0{,}006X_2X_3 + 0{,}073X_2X_4 - 0{,}257X_3^2 - 0{,}097X_3X_4 - 0{,}362X_4^2 \quad (3)$$

For tubular electrode wire LNM 420 FM:

$$B = 5{,}648 + 0{,}762X1 + 1{,}297X_2 - 1{,}416X_3 - 0{,}106X_4 + 0{,}054X_1^2 + 0{,}052X_1X_2 - 0{,}31X_1X_3 + 0{,}094X_3X_4 + 0{,}084X_2^2 - 0{,}36X_2X_3 + 0{,}95X_3^2 - 0{,}383X_4^2 \quad (4)$$

$$H = 2{,}389 + 0{,}784X_1 - 0{,}247X_2 - 0{,}908X_3 - 0{,}243X_4 + 0{,}061X_1X_2 - 0{,}192X_1X_3 + 0{,}228X_1X_4 + 0{,}250X_2^2 - 0{,}020X_2X_3 + 0{,}489X_3^2 - 0{,}103X_2X_4 \quad \text{.....} \quad (5)$$

$$K = 3{,}080 - 0{,}41X_1 + 0{,}379X_2 - 0{,}713X_3 + 0{,}101X_4 - 0{,}378X_1^2 + 0{,}168X_1X_2 + 0{,}192X_1X_3 - 0{,}133X_1X_4 - 0{,}039X_2^2 - 0{,}141X_2X_3 + 0{,}119X_2X_4 - 0{,}115X_3X_4 - 0{,}362X_4^2 \quad \text{.. ..} \quad (6)$$

Based on this study an optimal technological mode was defined with respect to productivity and quality, described by the parameters: current strength 250 A, arc voltage 21V, and welding speed up to 0,28 m / min.

Fig. 1 shows the graphic representation of the derived models. From them, except for the qualitative influence of the parameters, known from practice, the precise value of the studied parameter of quality can be defined for the corresponding electrode wire.

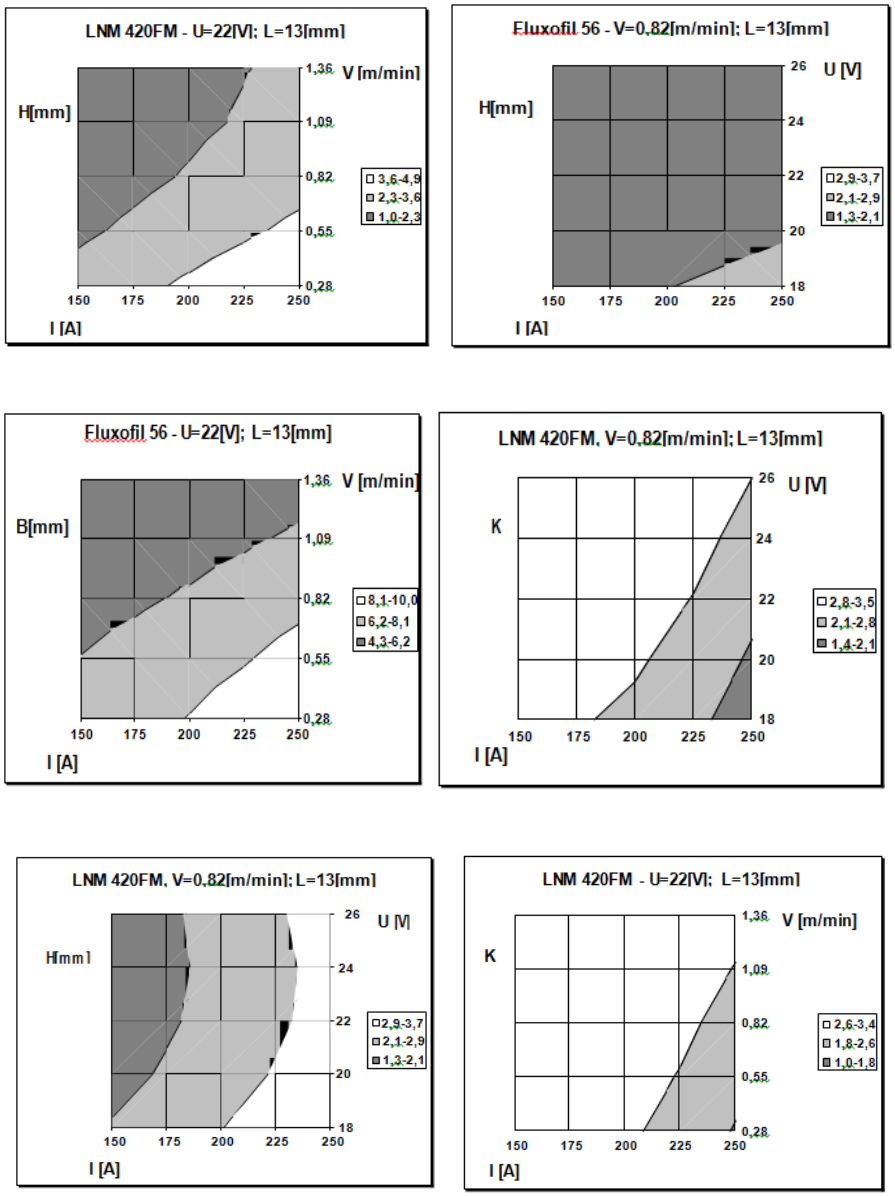

Figure 1. *Graphic images*

Welding seams about 9mm wide are produced with the help of the electrode wire FLUXOVIL 56 at voltage values higher than 33 V, values of the welding current exceeding 200A and velocities up to 0,55 m/min. Under these modes, however, the height of the seam for this type of electrode wire is no more than 2,5 mm.

Covering layers with bigger thickness up to 4 mm at the range mentioned above can be realized by means of LNM 420 FM.

Essential differences between the studied electrode wires were established during the analysis of the visual assessment of the seam quality at the various technological parameters. After conducting the experiment, expert assessment of the seam appearance was made by the three-level scale and

based on it the regression dependences 3 and 6 were derived. By means of the electrode wire LNM 420 FM considerably better quality of the welded seams is achieved at the used range of technological modes.

A particular recommended mode can be specified for the specific electrode wire from the realized graphic study depending on the user's requirements.

IV. Conclusions

Three regression equations have been derived for each of the two studied electrode materials, defining the influence of the technological factors (current, voltage, welding speed, electrode outlet) on the geometric and functional parameters of welded layers.

An optimal technological mode has been identified for deposition of layers with respect to their geometric and qualitative parameters.

References

[1] Antonov, V., Y.Kehayov.1986. Defining
[2] the kinematic parameters of the mode of welding for rotational details in a carbon dioxide medium, Rousse.
[3] Vassilev, V.1999.Technology of
[4] rehabilitation of details, Rousse University "Angel Kanchev".
[5] Ryabtsev, I., V. Kondratyev.1999.
[6] Mechanized electric arc welding of metallic equipment details, Kiev.
[7] Tonchev, N.1986. Modern technologies for details rehabilitation, Rousse.
[8] Vuchkov, I.1990. Identification of
[9] experimental studies, Techniques, Sofia.
[10] Tonchev, N, N. Kemilev, A. Monov.2004.
[11] Application of the Taguchi method in the field of welding in gas mixtures by means of tubular wires, 4th international scientific conference "Transport 2004", p.p. 297-300.

INVESTIGATION OF STATIC CHARACTERISTICS OF DIGITALLY-CONTROLLED ELECTROHYDRAULIC STEERING SYSTEM

Alexander Mitov[1], Jordan Kralev[2], Ilcho Angelov[3]

[1] TU-Sofia, Faculty of Power Engineering and Power Machines, dept.: „Hydroaerodynamics and Hydraulic Machines", e-mail:alexander_mitov@mail.bg
[2] TU-Sofia, Faculty of Automatics, dept.: „System and Control", e-mail:jkralev@yahoo.com
[3] TU-Sofia, Faculty of Power Engineering and Power Machines, dept.: „Hydroaerodynamics and Hydraulic Machines", e-mail:ilangel@tu-sofia.bg

Abstract*: The paper presents theoretical and experimental results for static characteristics of steering electrohydraulic system with digital control. Theoretical investigation is based on analytical mathematical models. Experimental results characterize static behavior of the system. They are executed on specially designed test rig for evaluation of electrohydraulic steering unit (EHSU). The purpose of experiments is to prove predictions of theoretical models.*

Keywords: Static Characteristics, Electrohydraulic Steering System, Digital Control;

Introduction

The main advantage of hydraulic drive system is their high density of power transmission with respect to their small dimensions. It is the main reason for their application in the field of industrial and mobile machines. Moreover, the ability for accurate position control allows their application in steering control of movement direction in various vehicles.

Increase in demand of such mobile machines with automatic control of working motions as well as trajectory direction is important factor for evolution of incorporated electrohydraulic steering systems. The key element in this system is electrohydraulic steering unit (EHSU).

EHSU with digital control are relatively new and not sufficiently researched technical solutions. Their functional behavior is strongly dependent on mechanical and electrohydraulic units as well as control system and embedded digital regulators. Therefore it is reasonable to investigate static and dynamic behavior of whole system composed of executive servo-cylinder, EHSU and digital control system [7].

The paper presents theoretical and experimental results for static characteristics of steering electrohydraulic system with digital control. Theoretical investigation is based on analytical mathematical models.

The main purpose is to experimentally prove and analyze the resultant from mathematical models static characteristics.

Experimental lay-out of investigated system

In department of "Hydroaerodynamics and Hydraulic Machines" of Technical University of Sofia is designed and implemented a test bench for EHSU type OSPE200 with displacement volume 200 cm^3. Implemented test rig for the present research is utilized for functional evaluation of EHSU. The test rig allows evaluation of EHSU in two modes:

- Mechanical – input control signal is generated from the steering wheel;
- Digital – input control signal is generated from electronic joystick.

Figure 1 shows a hydraulic diagram of test bench. Detailed description of its schematics and contruction can found in [6,7].

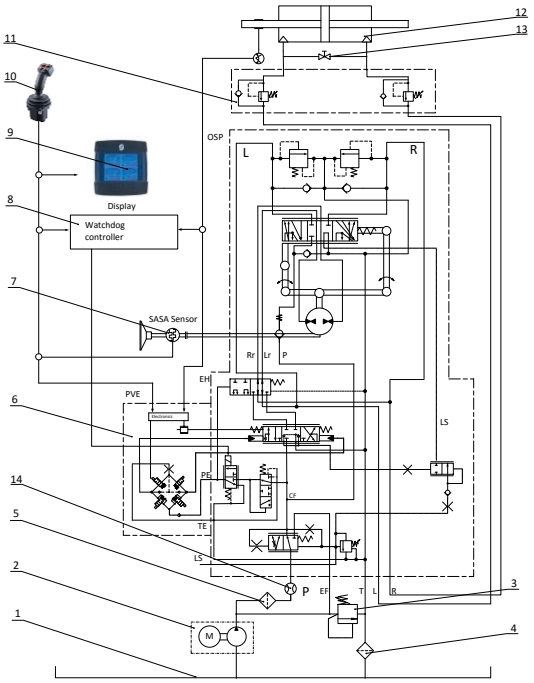

Fig.1. Hydraulic diagram of test bench

Mathematic modeling of static characteristics

Figure 2 shows the structure schematics of closed loop system for control of EHSU test bench. The system is composed of two loops – internal and external. Internal loop consists of local feedback (spool movement), PVE-block for digital control of EHSU and controlled internal spool/sleeve valve. External loop encloses reference signal (generated from joystick), programmable microcontroller, EHSU and

The outer loop covering global feedback consists of Reference (formed by joystick), a programmable controller EHKU and executive servo-cylinder. The output signal of the system is the position of the cylinder.

Mathematical modeling of internal loop

It is composed mathematical model of static characteristic, according to indications in Figure 2, internal loop of the closed system [7].

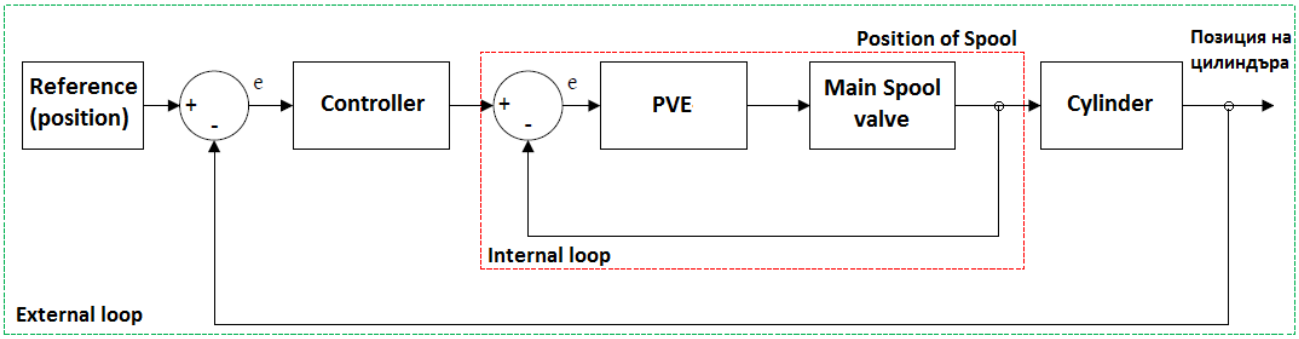

Fig.2. Structural diagram of the closed loop control system

Figure 3 shows a hydraulic diagram of electro proportional part of EHSU consisting of a four two-way, two position (2/2) valve connected in parallel and control hydraulic spool valve determining the direction of the executive servo-cylinder in digital mode [2].

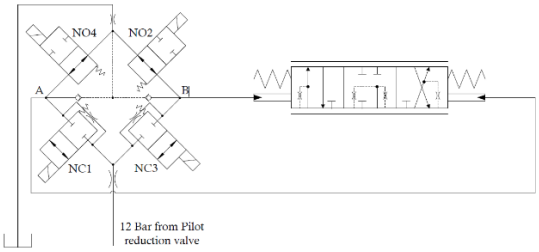

Fig.3. Hydraulic diagram of spool valve controlled by four solenoid valve

- Continuity equation for the two-way (NO-NC) valves.

$$q_{NO,NC} = \mu S_v \sqrt{\frac{2}{\rho}(p_1 - p_2)}, \ m^3/s, \quad (1)$$

where:

$q_{NO,NC}$ – flow rate thought 2/2 valves;

μ – coefficient of flow rate;

ρ – density of working fluid, kg/m^3;

p_1, p_2 – pressure in p.1 and p.2, Pa.

- Flow rate caused by the compressibility of the working fluid.

$$\frac{dp}{dt}\frac{V}{K} + \frac{dV}{dt} = q_{in} - q_{out}, \ m^3/s \quad (2)$$

$$\frac{dp}{dt}\frac{V}{K} + \dot{V} = q_{in} - q_{out}, \ m^3/s\ , \quad (3)$$

where:

V – initial volume, m^3;

K – bulk modulus, Pa

$\dot{V}$–flow rate caused by the compressibility,m^3/s;

q_{in}, q_{out} – flow of input and output of each of the 2/2 valves.

- Pressure drop in two-way two-position valves (NO-NC) valves.

$$\Delta p = \frac{K}{V}\int\left(q_{in} - q_{out} - \dot{V}\right)dt + p_i\,,\ Pa \qquad (4)$$

where:

p_i – is the initial value of pressure, Pa.

- Equation of force balance of the Main Spool.

$$\sum_{i=1}^{n} F_i = m_{sp}.\ddot{x}\,,\ N \qquad (5)$$

$$F_{pr.} - F_{spr.} - F_{fl.} \pm F_{fr} = m.\ddot{x},\ N \qquad (6)$$

$$F_{pr} = p_a.A_A - p_B.A_B \mp F_{fr}, \quad N, \qquad (7)$$

where:

m_{sp} – mass of the spool, *kg;*

$\ddot{x}$ – acceleration of the spool, m/s^2;

F_{pr} – pressure force on both sides of the spool, N;

$F_{spr.}$ – force of the spring, N;

F_{fr} – friction force, N;

$F_{fl.}$ – steady state flow force, N;

p_a, p_B – pressure in area A and B, Pa;

$A_A = A_B = A$ – area on both sides of the spool, m^2.

$$F_{pr} = (p_A - p_B).A,\ N \qquad (8)$$

- The force induced by the spring acting on the spool.

$$F_{spr} = -c.x_{sp} + F_{of.},\ N\,, \qquad (9)$$

where:

c – constant of the spring, N/m ;

$F_{of.}$ – force from preliminary spring deflection, N/m.

- Steady state flow force

$$F_{fl} = 2\mu.K_c.S.\Delta p.cos\theta,\ N \qquad (10)$$

- Equation of motion of the main spool valve.

$$F_{res}(t) = m_{sp}.\ddot{x}\,(t), \quad N \qquad (11)$$

$$\dot{x}(t) = \int \frac{F_{res}(t)}{m_{sp}} + \dot{x}(0)dt \qquad (12)$$

$$x(t) = \iint \frac{F_{res}(t)}{m_{sp}} + \dot{x}(0)dt + x(0)dt, \qquad (13)$$

where:

F_{res} – resultant force, N;

Mathematical modeling of the external loop of the closed system

Figure 4 shows a hydraulic circuit with the main indications of the parameters required for modeling the system with priority valve [2].

- Equation of force balance for a priority valve.

$$p_{CF}.A_{prior.} = p_{LS}.A_{prior.} + k_{spr.}.V_{sp.,displ.} \qquad (14)$$

$$p_{CF} - p_{LS} = \frac{p_{LS}.V_{sp.,displ.}}{A_{prior.}} = const\ , \qquad (15)$$

where:

p_{CF} – inlet pressure of EHSU, Pa;

p_{LS} – pressure in LS-line, Pa;

$A_{prior.}$- area of the spool of the priority valve, m^2;

$V_{sp.,displ.}$- volume in the priority valve , m^3.

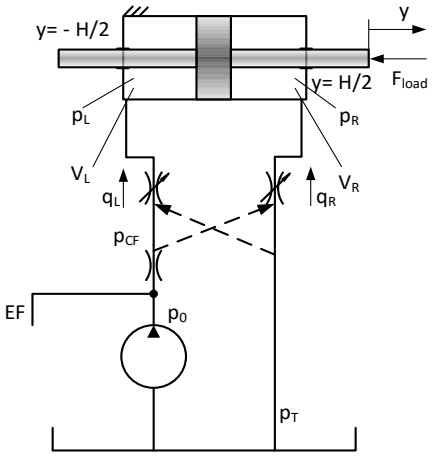

Fig.4. Hydraulic diagram of the system with priority valve and variables

- Continuity equation for throttling sections of the spool in the proportional valve to the left area of the executive servo-cylinder.

$$q_L = \mu S_{(x)} \sqrt{\frac{2}{\rho}(p_{CF} - p_L)}\, , m^3/s \qquad (16)$$

$$q_L = S_{(x)}.k_{orif.}, m^3/s \quad , \qquad (17)$$

where

$$k_{orif.} = \mu \sqrt{\frac{2}{\rho}(p_{CF} - p_{load})} \qquad (18)$$

Figure 5 shows the profile of the throttling sections in the proportional spool valve, the embodiment of which is described in detail [7].

range $0 \le x \le 0{,}3.10^{-3}$, *m*

$$S_1(x) = 1{,}83.n.\sqrt{R}.x^{\frac{3}{2}}, \qquad (19)$$

at $x = 0{,}3.10^{-3}$, follows $S_1(x) = ,043.10^{-12}\ m^2$

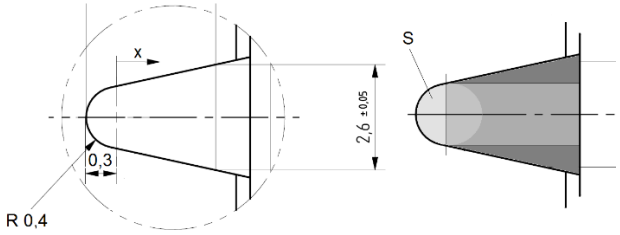

Fig.5. Throttle sections in the spool of proportional valve

range $0{,}3.10^{-3} \le x \le 3{,}5.10^{-3}$, *m*

$$S(x) = S_1(x) + 0{,}73.10^{-3}(x - 0{,}3.10^{-3}), \qquad (20)$$

Based on experimental data obtained and developed program [1] were obtained approximating analytical dependencies enabling change the coefficient of flow as a function of Reynolds number, μ = μ (Re).

In throttle section type "equilateral triangle":

- if $0 < Re \le 100$, то:

$$\mu_x = 5{,}938.10^{-4} + 8{,}586.10^{-3}.Re - 3{,}291.10^{-5}.Re^2 \qquad (21)$$

- if $100 < Re \le 2200$, то:

$$\mu_x = 0{,}592 + 1{,}492.10^{-4}.Re - 3{,}732.10^{-8}.Re^2 \qquad (22)$$

In throttle section type "circular cut-out":

- if $0 < Re \le 250$, то:

$$\mu_x = 3{,}741.10^{-3} + 3{,}282.10^{-3}.Re - 4{,}761.10^{-6}.Re^2 \qquad (23)$$

- if $250 < Re \le 6000$, то:

$$\mu_x = 0{,}50029 + 9{,}7903.10^{-5}.Re - 0{,}8725.10^{-8}.Re^2 \qquad (24)$$

- Equation flow supplied to the right chamber of the cylinder.

$$q_R = \mu S_{(x)} \sqrt{\frac{2}{\rho}(p_R - p_T)}\, , \ m^3/s \qquad (25)$$

$$q_L - \dot{y}.A_{cyl.} = \frac{V_L}{K}.\frac{dp_L}{dt} \qquad (26)$$

$$p_R = \int q_L - (\dot{y}.A_{cyl.})\frac{K}{A_{cyl}\left(\frac{H}{2}+y\right)}dt \qquad (27)$$

$$\dot{y}.A_{cyl.} - q_R = \frac{V_R}{K}.\frac{dp_R}{dt}\, , \qquad (28)$$

where $V_R = A_{cyl.}\left(\frac{H}{2} \pm y\right)$

$$p_R = \int (\dot{y}.A_{cyl.}) - q_R \frac{K}{A_{cyl}\left(\frac{H}{2}-y\right)}dt \qquad (29)$$

Presented dependencies mathematical model for internal and external loop (according to structural diagram in Figure 2) are adapted for different operating points of established regime. Based on those developed M-script file to calculate the static characteristic of the investigated system. Graphics depicting the result obtained theoretically static characteristic is shown in Fig.6.

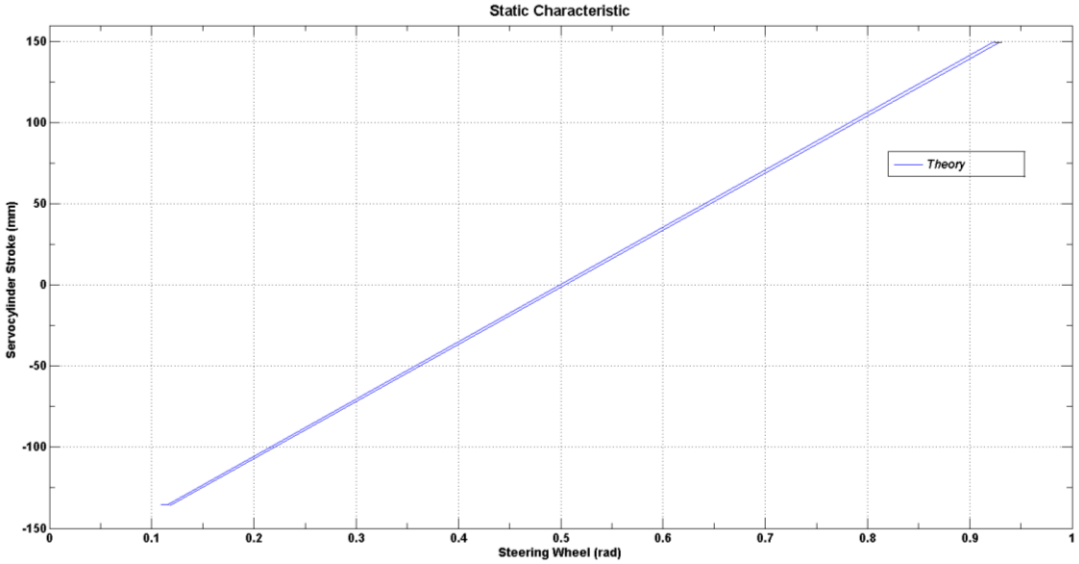

Fig.6. Theoretical static characteristic of the system

Experimental study of static characteristics

On Figure 7 shows two experimentally derived static characteristics of the investigated steering electrohydraulic drive system. One of them (OSP Subsystem) is obtained in hydro-mechanical control through spool/sleeve device in EHSU. The second of them (EH Subsystem) is obtained by counting the frequency of rotation of the steering wheel [6], respectively shaft by SASA sensor (pos.7, Fig.1)[8]. The measured signal is sent to the controller that generates a control signal to PVE-module for digital control.

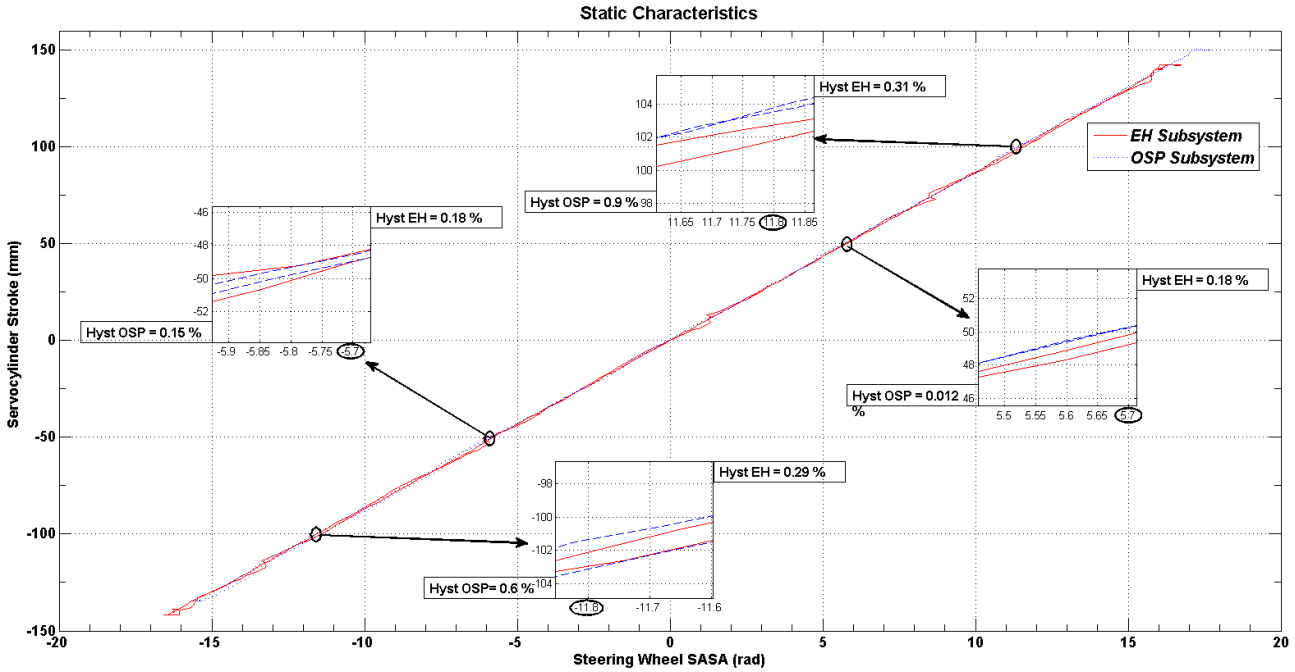

Fig.7. Experimental static characteristics of the system

The static characteristic presents the amendment of the position detected by feedback sensor of the cylinders as a function of angular rotation of the steering wheel in steady state [4,5].

An assessment and analysis of the quality of the static characteristics in terms of hysteresis. It is calculated by the formula (30), and the resulting values are shown on Fig.7.

$$H = \frac{|y_1 - y_2|}{y_{NOM}}.100, \%, \quad (30)$$

where:

y_1 - position of cylinder when steering to the right, mm;

y_2 - position of cylinder when steering to the left, mm;

y_{NOM} - nominal stroke of cylinder, mm.

Experimental studies were carried out at relatively low speeds (1 tr/min) [3], determined by the human operator to ensure the establishment of transitional processes. However, there are some overshoot in the dynamics that occur as local breakpoints in the static characterization (EH Subsystem).

Conclusion

Based on the results of theoretical and experimental studies of static characteristics there can be made the following important conclusions:

1. The estimated hysteresis in four symmetrical points compared to the average position of the cylinder proves the proximity of the two characteristics. There is an obvious correlation between theoretical and experimental result (Figure 6 and Figure 7).
2. In the case of control through the controller, the results depend on embedded software algorithm. The results for this case can be improved for example with application of more accurate model of the plant.
3. Due to the large number of units of the system and the complexity of the processes in it most appropriate approach for obtaining models is by means and methods of identification.
4. The linear nature of the static characteristic is the only prerequisite to argue that the system is linear dynamics. This is a reason to perform a research on both linear and nonlinear models with identification and control of the steering system.

Reference

[1] Angelov, Il. Investigate of pilot operated two way flow control valve from hydraulic drive system *for lifting devices of forklifts*, Dissertation, Technical University of Sofia, 1991.

[2] Bertelsen, D., C. Jeppesen, et. al., *Modelling and control of OSPE valve*, Aalborg University, Autumn, 2010

[3] Danfoss Inc.: *CAN in PLUS+1 Guide, Fundamentals of PLUS+1 Guide Electronics*, Training course, Almhult, Sweden, 2015.

[4] Fischer, E., A.Sitte, J.Weber,E.Bergmann, E.Motte. *Performance of an electro-hydraulic active steering system*, 10th International Fluid Power Conference (10thIFK`2016), Dresden, 2016.

[5] Harrer, M., P. Pfeffer. *Steering Handbook*, ISBN: 978-3-319-05449-0, Springer International Publishing, 2015.

[6] Mitov, Al., J. Kralev, Il. Angelov. *Digital Control Of Electro-Hydraulic Steering Test Bench*, МНК „Развитие на науката, технологиите и техниката за производство, опаковане, етикетиране, съхранение и дистрибуция на храни“, Journal of Food Packaging Science, Technique and Technologies, ISSN 1314-7773, Volume 7, Year 4, p.68÷73, Пампорово, 2015.

[7] Mitov, Al., *Research Of Steering Electrohydraulic Drive System With Digital Control*, Dissertation, Technical University of Sofia, 2016.

[8] Sauer-Danfoss Inc.: *OSPE Steering Valve SASA Sensor*, Technical Information, 11068682, Rev CD, Sep 2012.

INFLUENCE OF THE ELECTRIC ARC WELDING ON THE GEOMETRIC PARAMETERS OF ROTATIONALLY WELDED SEAMS BY A TUBULAR ELECTRODE WIRE

N. Hristov[1], I. Zumbilev[2]

[1]Todor Kableshkov University of Transport – Sofia
[2]TU-Sofia, Plovdiv Branch, izumbilev@mail.bg

Abstract: *This paper studies the influence of the electric arc welding in a shielding gas medium on the geometric parameters of rotationally welded seams by means of tubular and dense electrode wires. Regression models of the geometric parameters have been derived, and dependences have been built, reflecting the influence of the technological parameters on the controlled variables.*

Key words: welding, tubular wires, gas mixture

I. Introduction.

Rehabilitation of worn parts by welding is a promising trend in the economy of spare parts, raw materials and energy. Therefore rehabilitation of worn parts is widely implemented in the developed industrial countries and has a significant economic and ecological effect [2]. By means of welding the dimensions of the details can be restored, wear can be reduced, and surface layers with special properties can be deposited. Rehabilitative welding is with high economic efficiency. Complex and expensive details are is thus rehabilitated [5].

The electric arc welding in a shielding gas medium is one of the most widely used methods of rehabilitating worn details. Its advantages are high productivity, technological simplicity, equipment accessibility, and possibility for automation [4].

One of the prospective methods with wide area of application, combining high productivity with economic efficiency, is welding by means of tubular wires in a medium of shielding gas mixtures. The process of welding in shielding gas mixtures differs from the other types of welding in that the electric arc burns in a shielding gas jet, and the weld pool and the drops of the electrode metal are protected by the oxygen and the nitrogen in the air and in the gas medium, formed by this jet. One of the main advantages of the method is that with the help of alloying elements, welded metal with precisely defined properties can be deposited in the cores of bodies, which is difficult to achieve in the process of welding by dense wires. Except for alloying elements, gas-forming and slag-forming components are also introduced in the composition of the tubular wire, what ensures protection for the arc and proper performance of the physical and metallurgical processes in the area of welding.

The main parameters, influencing geometry and structure of the weld seam are the current, the voltage and the speed of welding. The quality of the welded layer in case of wide-layer welding greatly depends on the parameters of the single seams, of which it is composed [1].

The aim of this study is to derive regression dependences of the geometric parameters of rotationally welded seams, obtained by means of electric arc welding in a shielding medium composed of a gas mixture.

II. Materials and methods

The geometric parameters of the welded layer directly depend on the mode of welding, determined by the current strength I, the voltage U and the speed of welding $V_{weld.}$ The various combinations between them form the multiplicity of technological modes, leading to different geometry of the weld seam. Both the shape and the dimensions of the seam are directly related to the productivity in rehabilitating the worn surface and the quality of the welded layer.

A complete factorial experiment of 2^3 -type was conducted for achieving the goal. Samples from steel 40X were welded with the help of two types of electrode wires - Fluxofil 56 and LNM 420FM. The shielding gas mixture is gas corgon, comprising 82% argon and 18% CO_2.

Current X_1, voltage X_2, welding speed X_3 were used input factors, and the width B, the height H and the depth δ of the welded layer were taken as a target parameter. The range of variation of the control factors is given in Table 1.

Table 1. *Levels of variation and factors*

Levels	Control factors		
	X_1 Current [A]	**X_2 Voltage [V]**	**X_3 Welding speed [m/min]**
Lower limit (-1)	150	19	0,59
Basic level (0)	200	21,5	1,19
Upper limit (+1)	250	24	1,79
Range of varying	50	2,5	0,60

Each of the parameters of quality is controllable by measurement, in which it is quantitatively assessed in its own limited range of change.

The following equipment was used for conducting the experiments: source of current IZA – G 315; device for feeding the bodies UT-5; automat (tractor) for welding Kometa 2; gas burner RM 36M RZ2 - Imax- 360A (CO2); 320A ($Ar+CO_2$).

In order to achieve higher surface hardness of the welded layer at minimum area of thermal influence, the following components were chosen: tubular wire Fluxofil 56 – 1,4mm (produced by OERLIKON) DIN 8555, having the following chemical composition in weight percentage - C-0,35 , Mn-1,5 , Si-0,53 , S-0,007 , P-0,012 , Cr-5,2 , Mo-0,64; dense wire LNM 420FM (produced by LINKOLN), with the following chemical composition in weight percentage - C-0,45 , Mn-0,4 , Si-3 , Cr-9,5.

The adequacy of the models is defined by the coefficient of multiple correlation and confirmed by the calculated value of the F-criterion of Fisher, which needs to be higher than the tabular value.

The experiments were conducted with rotational test samples with diameter ∅ 38 mm and in accordance with the technologically possible speed, the change of the revolutions related to the speed of welding was defined after the formula

$$n = \frac{1000.V}{\pi.D}, \text{ where}$$

n – rotational speed (rev/min);

D – diameter of the sample (mm);

V – speed of welding (m/min)

The experiment was conducted with constant welding speed V=0,59 m/min. The single seams can be used to forecast achieving thicknesses at various velocities.

Each of the geometric parameters of the seam is described by a law of functioning in compliance, by which this parameter reacts to the action of the controlling factors.

The main task of every multi-factorial study reduces to studying the described problem by means of identification and mathematical description. From the initial information the studied parameters of quality have an explicit non-linear character with respect to the studied factors.

The adequacy of the models is defined by the coefficient of multiple correlation and confirmed by the calculated value of the F-criterion of Fisher, which is needed to be higher than the tabular value.

Table 2. *Levels of variation and factors*

Levels	Control parameters		
	X_1 Current [A]	**X_2 Voltage [V]**	**X_3 Step [mm]**
Lower limit (-1)	150	19	2
Basic level (0)	180	21	3
Upper limit (+1)	210	23	4
Range of varying	30	2	1

III. Results and discussion

After applying a standardized methodology [3], regression models of the geometry of the welded single layer were derived. From the preliminary experiment with changing the factors in accordance with Table 1, where B and H are measured in mm and represent respectively the width and the height

of the welded single layer for both types of electrode wires, the following dependences were obtained:

For the electrode wire FLUXOFIL 58:

$B\ (V, I, U) = 5{,}514 - 0{,}111.X_1 + 0{,}35.X_2 + 0{,}8.X_3 + 0{,}541.X_1^2 - 0{,}36.X_1.X_2 - 0{,}1.X_1.X_3 - 0{,}017.X_2.X_3 - 0{,}099.X_3^2$;

$H\ (V, I, U) = 1{,}426 - 0{,}012.X_1 + 0{,}268.X_2 - 0{,}119.X_3 - 0{,}032.X_1^2 - 0{,}252.X_1.X_2 - 0{,}331.X_1.X_3 + 0{,}289.X_2^2 - 0{,}189.X_2.X_3 - 0{,}016.X_3^2$;

For the electrode wire LNM 420 FM:

$B\ (V, I, U) = 5{,}418 - 0{,}098.X_1 + 1{,}198.X_2 + 0{,}38.X_3 - 0{,}052.X_1^2 - 0{,}107.X_1.X_2 + 0{,}151.X_1.X_3 - 0{,}325.X_2^2 - 0{,}146.X_2.X_3 - 0{,}219.X_3^2 - 0{,}617.X_1^3 - 0{,}654.X_2^3 + 0{,}232.X_3^3$;

$H\ (V, I, U) = 2{,}112 - 0{,}029.X_1 + 0{,}348.X_2 + 0{,}051.X_3 - 0{,}024.X_1^2 - 0{,}136.X_1.X_2 + 0{,}184.X_1.X_3 - 0{,}134.X_2^2 - 0{,}142.X_2.X_3 + 0{,}174.X_3^2 - 0{,}426.X_1^3 - 0{,}085.X_2^3 + 0{,}179.X_3^3$.

Regression dependences were also derived for the main experiment, whose parameters change according to Table 2. Based on them, the relationship between the thickness of the welded layer δ and the current value, the voltage, and the step can be defined. All derived dependences are adequate to a coefficient of multiple correlation close to 1 and the calculated criterion of Fisher, which is bigger than the tabular value.

For the electrode wire FLUXOFIL 58;

$\delta\ (I,U,s) = 1{,}485 + 0{,}0574.X_1 + 0{,}0015.X_2 - 0{,}44.X_3 + 0{,}113.X_1.X_2 + 0{,}1.X_1.X_3 - 0{,}072.X_2.X_3 + + 0{,}314.X_3^2$ **;**

For the electrode wire LNM 420 FM:

$\delta\ (I,U,s) = 2{,}953 + 0{,}714.X_1 + 0{,}046.X_2 - 0{,}9.X_3 + 0{,}021.X_1^2 - 0{,}123.X_1.X_2 - 0{,}116.X_1.X_3 + 0{,}043.X_2^2 - 0{,}040X_2.X_3 + 0{,}07.X_3^2$

Fig. 1 shows a graphic interpretation of the change of the thickness of the welded layer δ depending on the various technological parameters in the process of welding with the help of both types of electrode wires (the tubular FLUXOFIL 58 and the dense LNM 420 FM).

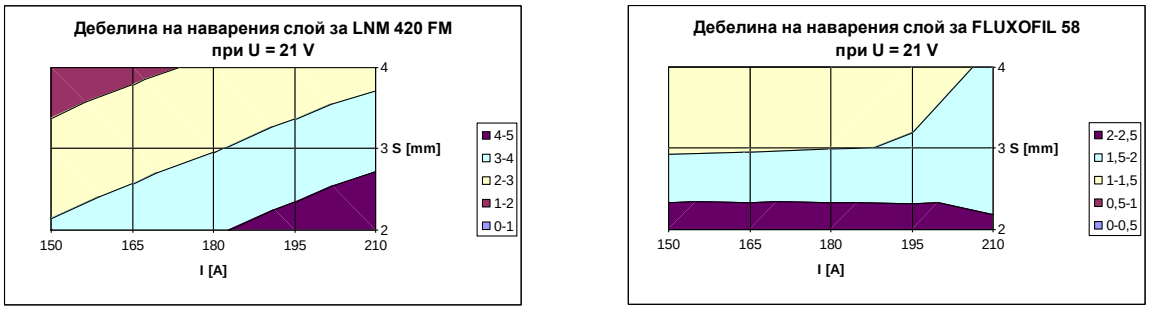

a b

***Figure 1**. Change of the thickness of the welded layer depending on the parameters of welding: a – for the electrode wire LNM 420 FM, and b – for the electrode wire FLUXOFIL 58*

As it can be seen from the graphs, considerably bigger welded layer can be achieved by using the dense electrode wire. The thickness of the welded layer can be forecasted based on the graphs, depending on the technological parameters of the process of welding.

IV. Conclusions

Mathematical models for rotationally welded seams have been derived that reflect the dependence between the technological factors (current strength, voltage, welding speed) and the target parameter – width, height, and thickness of the welded layer.

References

[1] Antonov, V., Y.Kehayov.1986. Determining the kinematic parameters of the mode of welding for rotational details in a carbon dioxide medium, Rousse.
[2] Vassilev, V.1996. Technology of rehabilitation of details, Rousse University “Angel Kanchev”,
[3] Vuchkov, I.1990. Identification of experimental studies, Techniques, Sofia,
[4] Ryabtsev, I., V. Kondratyev.1999. Mechanized electric arc welding of metallic equipment details, Kiev.
[5] Tonchev, N.1996. Modern technologies for rehabilitation of details, Rousse.

STUDY OF INPUT COLOURING AGENTS IN SOFT DRINKS

M. Petrova, I. Kostova, I. Ivanova, S. Damyanova, N. Vasileva

Department of Biotechnology and Food Technologies, University of Ruse "Angel Kanchev", BranchRazgrad, Aprilsko vastanie Blvd. 47, Razgrad 7200, Bulgaria,
e-mail: mgpetrova@uni-ruse.bg

Abstract: *In this study was done a research of the content of the labels of 101 soft drinks and it concerns the colouring agents used in their production. The aim is analyzing the role of labeling for the ordinary consumers to achieve an informed choice of soft drinks in its striving for healthy and balanced died.*

Key Words: food labels, soft drinks, colouring agents, consumers, information.

I. Introduction

Recently because of various reasons there is a decrease in the production of milk and dairy products in our country. The consumption of soft drinks, coffee, etc. is increasing especially among the younger generation. Soft drinks like "coca cola" without belittling their invigorating effect contain in an unit volume more calories than skimmed milk [1].

Can soft drinks be a part of healthy died of Bulgarians and be a factor in the balanced lifestyle? Do the packagings of soft drinks in Bulgaria give the necessary information about used raw materials and their functionality and if the information is understandable and acceptable? How can consumers be informed about the content or the absence of calories, to calculate the tentative daily take of sugar or to get acquainted with the health and nutritional benefits of consuming the product as well as for any damages? Can it be tracked which of the companies producing soft drinks on Bulgarian market have realized their responsibility to consumers and comply with regulatory requirements, implementing the best practices and systems for food safety?

The systems for quality management of food safety generally contain three components: Quality management system (QMS); Hazard analysis and critical control point system (HACCP); Preliminary programs and best practices [3].

Recently the range of drinks on the market is expanding based based on new tastes and flavors, there is a variety of energy drinks, drinks with vitamins, mineral supplements for sportsmen and others [2].

In this work it was done a study of the information from the labels of 102 soft drinks selected at random from the market. Based on the data from collected and processed labels we have analyzed the extent to which the consumers can make an informed choice of drinks.

II. Materials and methods

To conduct the study was used an electronic application developed with the program MS Excel Figure 1. It keeps the database of information of the collected labels of soft drinks. In the electronic data processing was used the rich functional and computing apparatus of the program MS Excel. As a basis for the study was used the information about contained additives in the drinks that can affect on a state of health: colouring agents, preservatives, antioxidants, thickeners, stabilizers, emulsifiers, sweeteners, etc.

The choice of soft drinks' labels was approached by accident together with a variety of range of soft drinks. It was given a slight priority of the drinks preferred by young people as well as those intended for children and elderly people.

The data processing was used the code set of values which greatly facilitates the use of buid- in functions in the program MS Excel. The wide variety of graphics of MS Excel provides an opportunity to demonstrate the various results of the study.

III. Results and discussion

The information about the origin of the tested soft drinks is given in Table 1 and shows the the soft drinks are mainly from Bulgaria (86%) and 8 more countries.

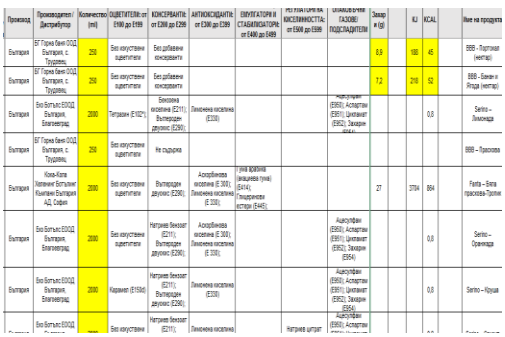

Figure 1

Table 1

Origin	Number of drinks
Bulgaria	88
Poland	1
Serbia	1
Romania	2
Turkey	4
Germany	1
Hungary	2
Romania	1
Korea	2

Additives can be used in foods for different purposes.

The classification of Codex Alimentarius divides additives into several groups: colouring agents (E100 – E199), preservatives (E200 – E299), antioxidants and acidity regulators (E300 – E399), stabilizers, emulsifiers, mineral salt (E400 – E599), additives enhancing the flavor (E600 – E699), antifoaming, glazing, flour improvers, sweeteners (E900 – E967) and ferments preparations (E1100 – E1105).

Among the regulated main groups with a technology function, a subject of this study are the colouring agents. They enhance or restore the colour of products. Colouring agents are natural constituents of products that can be extracted from them or can be prepared synthetically [5].

In toxicological terms synthetic colouring agents are not harmless to people or therefore Joint Expert Committee on Food Additives FAO and WHO monitors their application. The additives should be used primarily for restoring or enhancing the natural colour and to expand the opportunities to create a natural colour tone.

On Figure 2 can be seen the number of the colouring agents used in the tested soft drinks according the information on the labels. The processed data in percentages indicate that no artificial colouring agents are 40 % , 37 % of the soft drinks have a coloring agent, in combination with 2 to 5 artificial colouring agents are 22 %. 1% of the tested drinks there is no presence of used colouring agents.

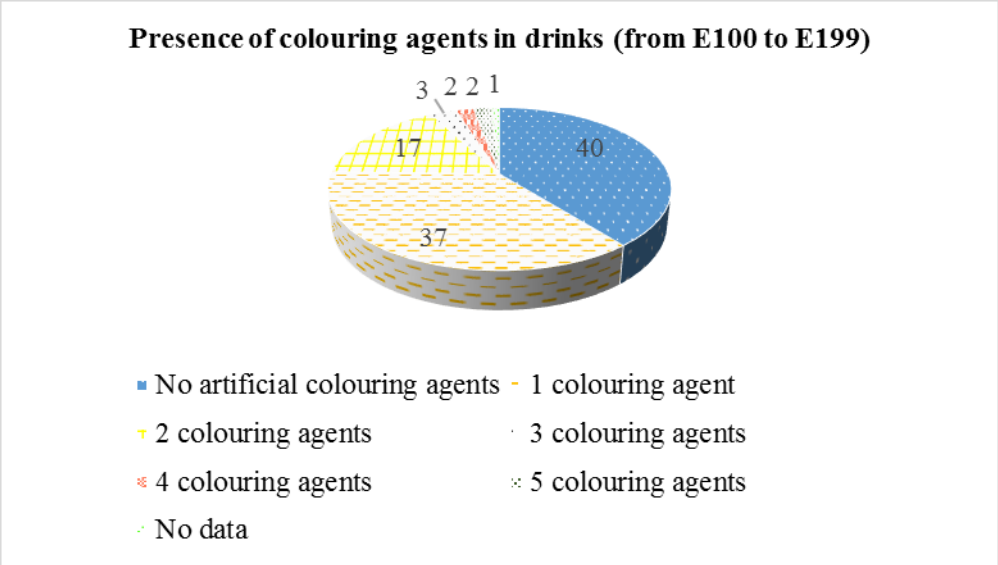

Figure 2

Figure 3 shows the information about the type and a number of the colouring agents in the tested soft drinks. The data in Table 2 represent the E-numbers of each colouring agent, its name and origin. It was given an assessment of their influence on the basis of literature data. For the purpose of achieving greater clarity in the table are used colour schemes resembling “traffic lights”. Obviously more artificial colouring agents can cause allergies, hyperactivity, indigestions, tumors [7].

Mixing of various synthetic colouring agents allows to achieve a colouring which can not be obtained with one colouring agent. The correct dosage of synthetic colouring agents depends on the colour, desired intensity of the colouring, the physicochemical properties of the coloured products and the specifics of the technological process.

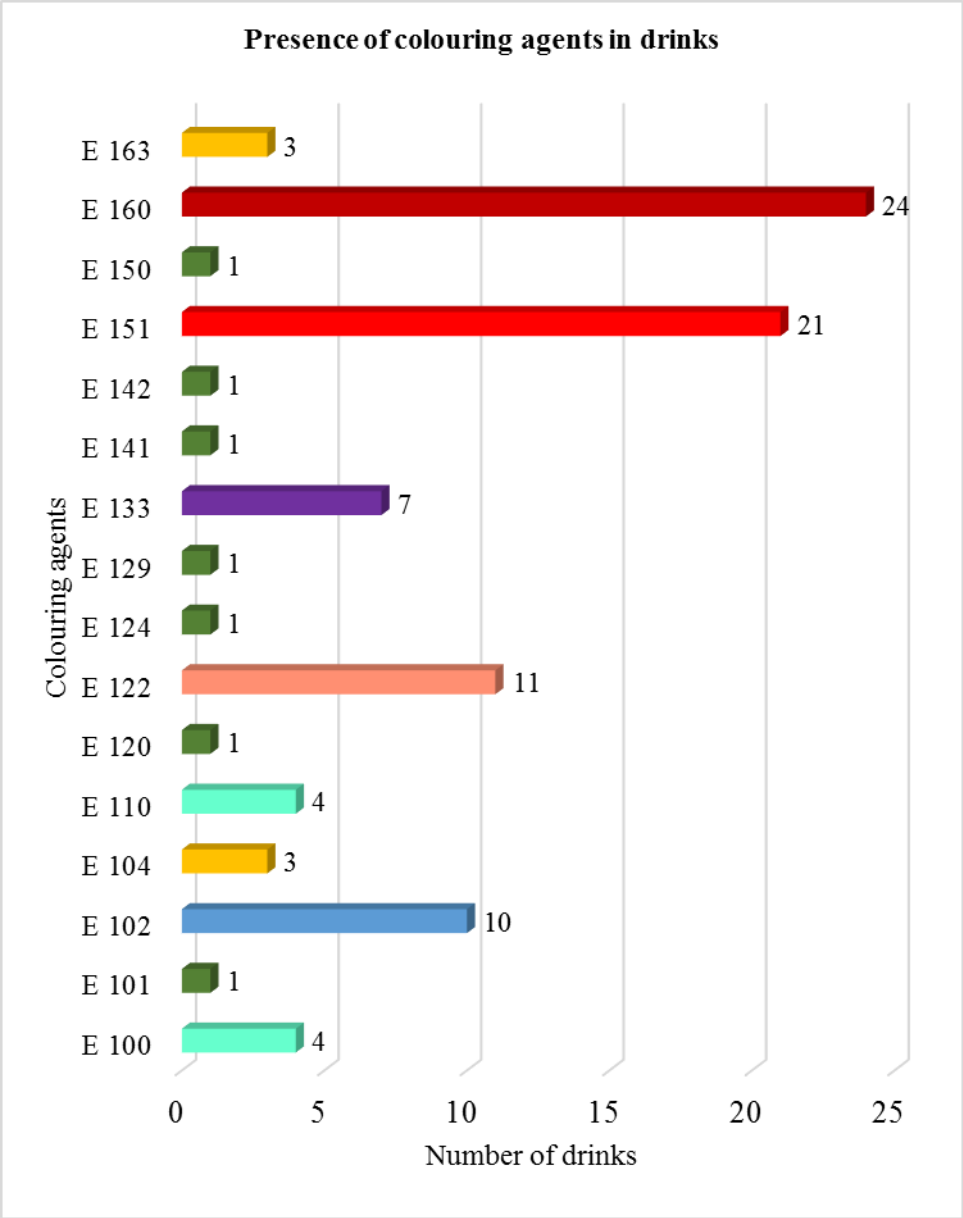

Figure 3

Table 2

E№	Name	Origin	Assessment
E 100	Curcumin, Turmeric	Natural pigment from yellow root (turmeric)	Harmless
E 101	Ribofllavin- Lactoflavin	Vitamin B2, occurs naturally in a lot of foods	Harmless

E 102*	Tartrazine	Artificial colouring agent	Often causes allergies in asthmatics and spirin-sensitive people. Provekes asthma attacks and urticarial among children. There is a connection to thyroid tumors, chromosomal da-mage, rashes and hyper-activity.
E 104	Quinoline yellow	Artificial colouring agent	Possibly causes allergies. Causes dermatitis. Banned in Australia, USA and Norway
E 110	Orange- Yellow S- Sunset yellow	Artificial colouring agent	Often causes allergies in asthmatics and spirin-sensitive people urticaria, rhinitis, nasal congestion, allergies, hyperactivity, kidney tumors, chromo-somal damage, abdominal pain, nausea and vomiting, indigestion, distaste for food. It was found increase of tumors in Banned in Norway.
E 120	Kohenil	Natural colouring agent	Possibly causes allergies
E 122	Carmoisine, Azorubine	Artificial colouring agent	Often causes allergies in asthmatics and spirin-sensitive people. Banned in Sweden, Austria, USA and Norway.
E 124	Cochineal red	Artificial colouring agent	Like amaranth often causes allergies. In animals drives to formation of tumors. Banned in USA and Norway
E 129	Allura red	Artificial colouring agent	It was found its connection with tumors in mice. Banned in Denmark, Belgium, France, Germa-ny, Switzerland, Sweden, Austria and Norway
E 133	Brilliant blue	Artificial colouring agent	In large quantities can damage the kidneys and lymphatic vessels. Banned in Belgium, France, Germany, Switzerand, Sweden, Austria, Norway.
E 141	Combination of cooper and chlorophyll	Natural colouring agent of chlorophyll	No evidence of adverse effects
E 142	Green S	Artificial colouring agent	harmless Banned in Sweden, USA and Norway.
E 150	Caramel ordinary	Produced by heating sugar	harmless

E 150d	Caramel	Artificial colouring agent	Harmless in normal quantities
E 151	Brilliant red	Artificial colouring agent	May cause allergies Banned in Denmark, Australia, Belgium, France, Germany, Switzerland, Sweden, Austria, USA, Norway.
E 160	Carotene, derivated from carotene (E160a)	The most often of plants, sometimes naturally identical	Harmless
E 160e	Beta-apo-8-carotenal	The most common of oranges, intestines, liver, sometimes artificial	Harmless
E 163	Anthocyanins	Natural colouring agents of grapes, elderberries, red cabbage and granberries	Harmless

If we do a classification of soft drinks according their production technology we can group them into two main groups: carbonated and non- carbonated soft drinks. In the different types of soft drinks the content of sugar and dry matter is between 6,3% and 12,8%. The carbon dioxide content is more than 0,35% and the term of duration is from 6 days to one year [6]. Energy drinks called refreshing drinks represent liquids that give the body a quick supply of energy. But very many people are aware of the composition and effect of these drinks on the body and it is good to regarded as a particular kind. A number of studies show that the proportion of the students who consumer energy drinks is higher that the statistics for the country [2].

In Figure 4 it can be seen the number of studied labels depending on the type of a drink.

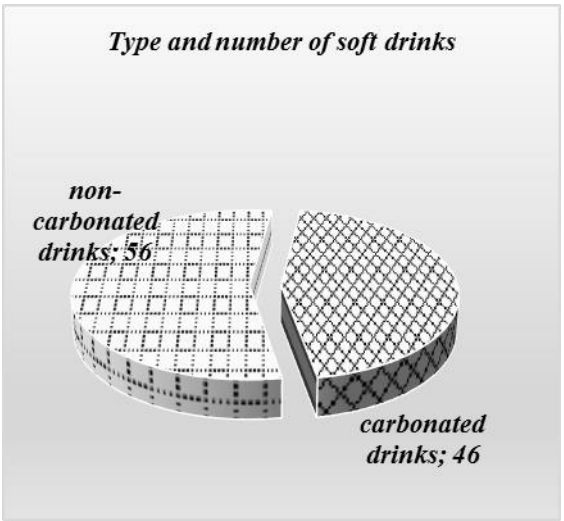

Figure 4

Figure 5 presents data about the drinks with no colouring agents in their composition. 50 % of non-carbonated drinks and 26 % of carbonated ones do not contain this type of an additive.

In the food industry synthetic colouring agents are used individually or in combination with other. The type of drinks with one colouring agent and their number is shown in Figure 6. It can be seen that one colouring agent was used in 25 % of non- carbonated drinks and in 48 % of carbonated ones.

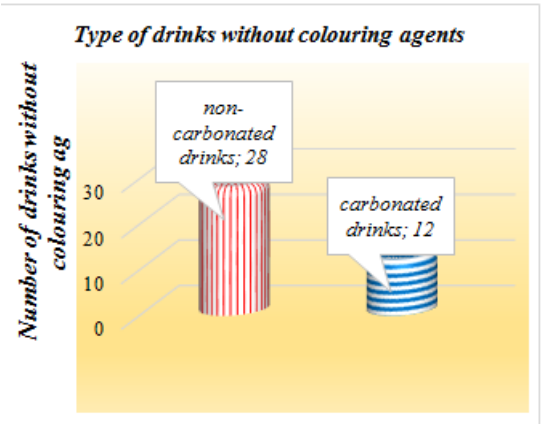

Figure 5

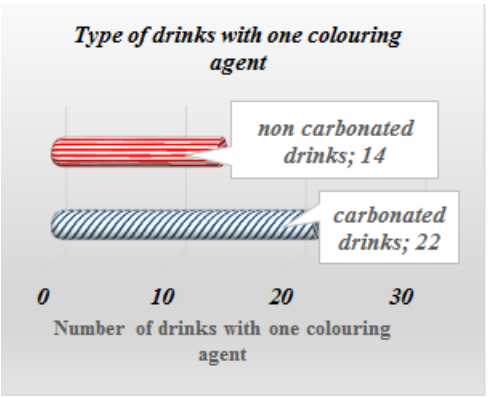

Figure 6

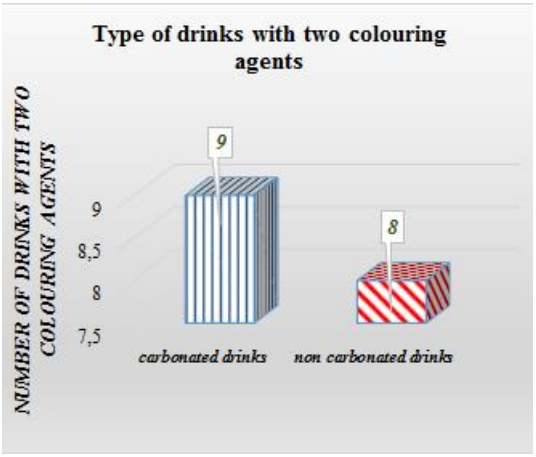

Figure 7

The type of the drinks with two colouring agents and their number is shown in Figure 7. Two colouring agents were used in 14 % of non-carbonated drinks and in 20 % of carbonated ones.

In Figure 8 it can be seen that the combination of three colouring agents was used in 7 % of carbonated drinks and in 2 % of non- carbonated ones.

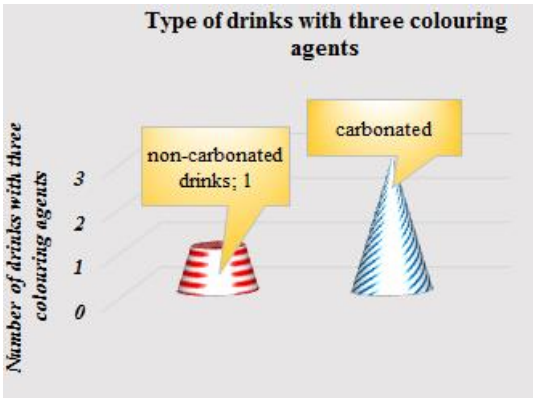

Figure 8

In 4 % of non- carbonated drinks were used more than 3 colouring agents.

IV. Conclusions

The conducted study about the input colouring agents in soft drinks shows that they are used individually as well as in combination to achieve the required intensity of colouring. The data point that the artificial colouring agents are not harmless and it is necessary to make a careful choice of soft drinks in our daily lives. Better consumer information will improve the culture of shopping and lifestyle. For this purpose we recommend the used additives to be noted on labels including colouring agents with the colours of a "traffic light" according to the degree of their effect on the health.

It is also recommended to carry out activities aimed at building a family and social environment for a healthy lifestyle including an informed choice of food and drinks.

References:

[1] Dimitrov T., S. Boycheva, N. Naydenova, Significance of milk and dairy products for a human being, Proceedings of Ruse University, 2008, v. 47, s. 8, 34-42.
[2] Koshevaya, V., Z. Romanova, Selection of natural flavor enhancers for the preparation of soft drinks, National University of Food Technologies, www.dspace.nuft.edu.ua/jspui/bitstream/123456789/9725/1/16.pdf.
[3] Vladimirov Zh., N. Malamova, C. Kovacheva, O. Harizanova, I. Kacarski, Implemention of Europian standards for quality and food safety in Bulgaria (Economic and social effects), Sofia, 2008, SU „St Kl. Ohridski", pp. 367, ASBN 978-954-9399-09-7.
[4] http://babh.government.bg/
[5] http://e-learning.uni-ruse.bg
[6] http://www.bb-team.org/
[7] http://www.mendov.eu/

STUDY OF THE ORIGINATION AND PROPAGATION OF CRACKS IN NITRIDED STEELS BY ACOUSTIC EMISSION

A. Zumbilev, I. Zumbilev

Technical University of Sofia – Branch Plovdiv, BULGARIA

Abstract: *The aim of the present paper is to study the possibility to use acoustic emission for studying the processes of crack formation in nitrided materials.*

The obtained results show that the acoustic emission can be used as an indicator of pre-fracture processes in nitrided details. It has also been established that two types of acoustic-emission activity are observed during the process of fracture in nitrided materials.

Key Words: acoustic emission, fracture, nitriding**.**

I. INTRODUCTION

Ion nitriding is widely used in modern mechanical engineering for improving the exploitation properties of tools and details. Nitrided details can be conveniently regarded as multilayer materials, composed of a matrix, a diffusion zone and a thin nitride (white) layer on the surface, which differ in chemical composition, parameters of their crystal lettuce, physical and mechanical properties[1,3]. These differences lead to origination of an additionally stressed state at the border matrix - diffusion zone – combined (nitride) zone. If, during exploitation, the overall stresses in an arbitrary cross-section exceed the values of the critical stresses of de-cohesion for a given multilayer system, then brittle fracture will start in exactly in these boundary sections or zones [1,3,5].

Since the nitride layers are characterized by a high elasticity modulus, the stresses, occurring in them at certain deformation, are considerable, and the availability of defects in their structure, are factors, favoring the origination of microcracks.

Papers [13,14,15,16] describe a number of methods for studying the processes of origination and propagation of cracks in multilayer systems. A common flaw of these methods is the fact that they are applied after completion of the process of fracture.

One of the most modern methods for studying the processes of microcracking and fructure in the matrix and its thin layers is the acoustic emission [2,4,13,14,15,16]. Acoustic emission of impulse type is observed in materials, when mechanical energy of elastic deformation is released at the moment of microcracking or crack propagation. Energy is released in the deformed material discreetly, as a series of individual acts, registered as AE-impulses and AE-events in a minor volume of the material. They are then propagated in the form of waves of elastic deformation (stress waves, AE-waves) throughout the volume. Registration of the spectrum and the parameters of AE, radiated by a material, subjected to deformation, gives important information about the mechanisms of the process of microcracking and fracture of nitride materials.

The aim of the present paper is to study the possibility to use acoustic emission for studying the processes of microcracking and fracture in nitrided materials.

II. METHODOLOGY OF STUDY

Experimental studies were conducted with steel BH11 BS4659 (4Х5МФС - ГОСТ), from which standard test samples were made [9,10] with a notch for three-point bending – Fig. 1. The top of the notch was made by a thread electro-erosive machine with a radius of curvature of 0,09 mm and a length of 5 mm. It was proved by metallographic analysis that after subjecting to the process of nutriding, the top of the notch was not nitrided.

The spherical waves, radiated by the source, were transformed into surface AE – waves (stress waves), and registered by the sensor (2), attached to the sample (1). The mechanical energy of the acoustic-emission impulse was converted into an equivalent electrical signal. After filtration, it was fed into the pre-amplifier and then to the analogue part for additional amplification and processing by the computer block of the AE-equipment PAC 3000/3104" (3). The characteristics of an AE-signal (duration, time of increase, impulses, amplitude, energy etc.) were processed by the microcomputer of the AE system and could be printed on a printer (4). The experiments were conducted at room temperature.

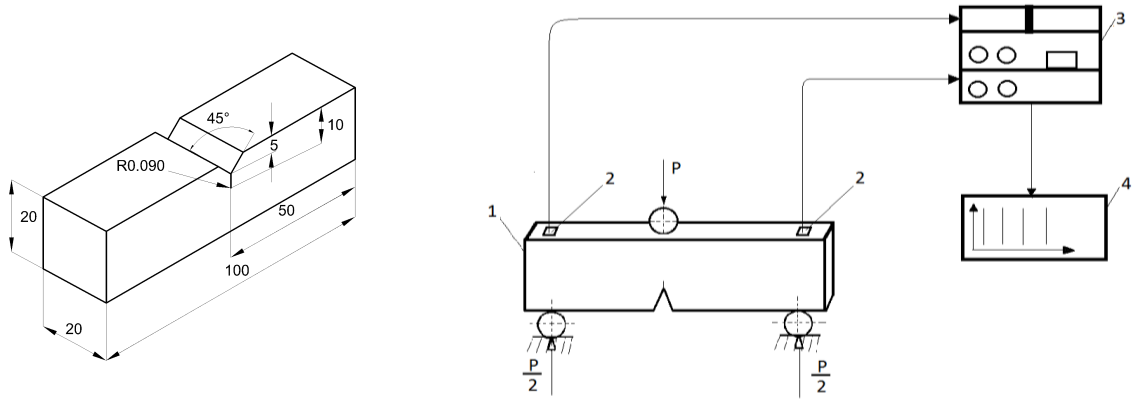

a b

Figure 1. *a – test sample, b – block-scheme of the experiment*
1-sample, 2-sensors, 3- AE system - PAC 3000/3104, 4-printer

The samples were thermally treated in a vacuum furnace VKUQ - Degussa, and then part of them were subjected to ion nitriding in the installation ION-20. After the thermal treatment the samples were grinded at R_a = 0,32 μm. The modes of thermal treatment and ion nitriding are given in Table 1.

Table 1. *Modes and results from the ion nitriding of steel BH11*

№ Of the sample	t_{hard} °C	$t_{temp.}$ °C	HRC	$t_{nitr.}$ °C	P_{NH3} Pa	τ h	$HV_{0.1}$	$\delta_{tot.}$ μm	$\delta_{c.z.}$ μm
215	1040	600	51	530	300	7	1168	240	6
249	1040	650	46	530	300	10	1100	270	8

It was proved by metallographic and fractographic analysis that the tip of the notch was not nitrided after nitriding.

The resistance against crack propagation was defined for three-point bending of the samples by means of a universal testing machine INSTRON 1343 at speed of loading 0,5mm/min. The displacement of the crack banks (V_9) was registered at room temperature by a console tenso-resistive perceiver with sensitivity 2,5 μV/mm, base 10 mm and step 2 mm, and the diagram force- banks motion was recorded at the same time.

For studying the AE-activity in case of three-point bending and fracture of the samples, a four-channel AE system PAC 3000/3104 with wide-band sensors Wd was used - Fig. 2. The sensors were placed on a sample, locally doped with silicon paste, and fastened with special springs, providing constant pressure. The sensitivity of the sensors was controlled by the imitator of Xcy. At total amplification of 80 dB (40 dB pre-amplification) and constant threshold of 1V, a registered signal of 98 dB from the imitator was taken as good sensitivity.

For clearing out and correct interpretation of the results from the acoustic-emission (AE) tests, calibration curves were obtained based on metallographic and fractographic analyses, concerning the different structural states.

The obtained graphical and tabular AE-information was cleared at the maximum from the influence of noises by appropriate conduction of the experiments and consequent data analysis.

III. EXPERIMENTAL RESULTS AND ANALYSIS

The acoustic-emission parameters: AE-impulses (C), rise time (RT) and pressure (P) are shown in dependence on the displacement of the crack banks (V_9) – Fig.2.

The experimental results from the acoustic-emission activity of the ion nitride samples (215, 249) speak of brittle fracture with clearly expressed character and are presented in Fig. 2 and Fig. 3.

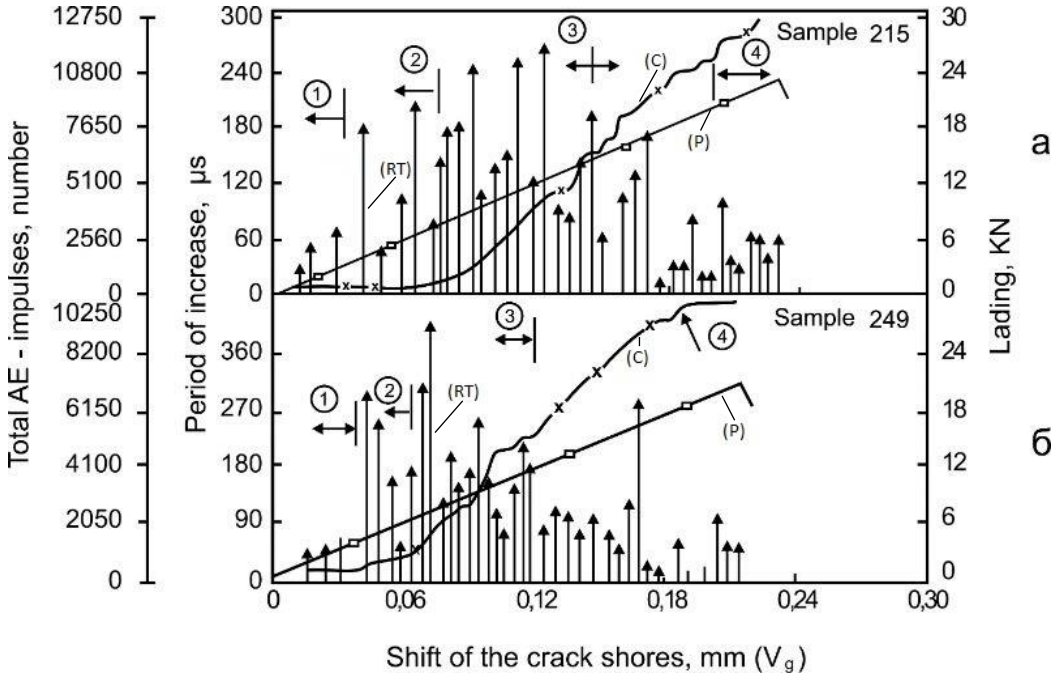

Figure 2. *Change of the AE-parameters and the load with respect to the displacement of the crack banks for the ion-nitrided samples 215 and 249*

The fracture of the ion-nitrided samples is in the linear elastic zone of the curve P-V_9.

The AE-activity of the samples is with considerably lowered AE-parameters at low loads. Fig. 1, number ① denotes this zone of low AE activity, in which the rise time of the registered AE phenomena is below 60μs, and the AE-impulses are with low intensity. The AE-phenomena, registered in zone ① are due to premature microcracking of the layer, when the deformation at small loads is sufficient to achieve the critical destructive stresses for the imperfect (defective) micro-sections of the layer [1,3]. This confirms the assumption that these stresses do not necessarily lead to microcracks in the matrix. The assumed micro-cracking in the defective sections of the layer is also supported by the fact that the layer has a significantly higher modulus of elasticity and it will crack before the tensile strength of the matrix is reached.

In the three-point bending processes of reduction of the residual compressive stresses occur. This is also accompanied by plastic deformation of the layer. The formation of a zone of plastic deformation in front of the crack tip and in the layer is the reason for the observed AE-activity in zone ② Fig.2. It is with comparatively high values of rise time. In the third zone ③, characterizing mainly the processes of brittle fracture of the matrix, linear rise of the total number of AE-impulses is observed. This type of distribution of the AE-impulses is characteristic of the processes of fracture, evenly distributed in time or with respect to the load and containing elements of ductile fracture. It is possible to isolate a fourth zone ④ in the studied samples, where the AE-activity is with lowered parameters again. It corresponds to the final brittle micro-cracking of the layer and the fracture of the whole sample.

For the cumulative distribution of the AE-energy four zones can also be distinguished, what confirms the assumed behavior at fracture, causing the corresponding AE-activity – Fig. 3.

It can be noted in conclusion that two types of AE-activity are observed in the studied samples. They are characterized by four zones of AE-activity: zone of premature microcracking of the layer; zone of plastic deformation in front of the notch tip; zone of brittle fracture of the matrix and zone of final microcracking and fracture of the sample.

The AE-activity can be used as an indicator of pre-fracture processes in nitride details and tools.

Based on the carried acoustic-emission and fractographic analysis, the following probable mechanism of fracture of a nitrided body, subjected to static loads, is suggested.

At low initial pressure (P) of the ion-nitrided sample - up to 6 KN - in front of the notch tip at both its ends, where a nitride layer is present, processes of reduction of the residual compressive stresses occur, on the one hand, and, on the other hand, premature

deformation of the layer and its microcracking occurs due to its high modulus of elasticity – Fig. 2, zone ①**.** Microcracks are formed first in the combined (white) zone and then in the diffusion zone (Fig.4a).

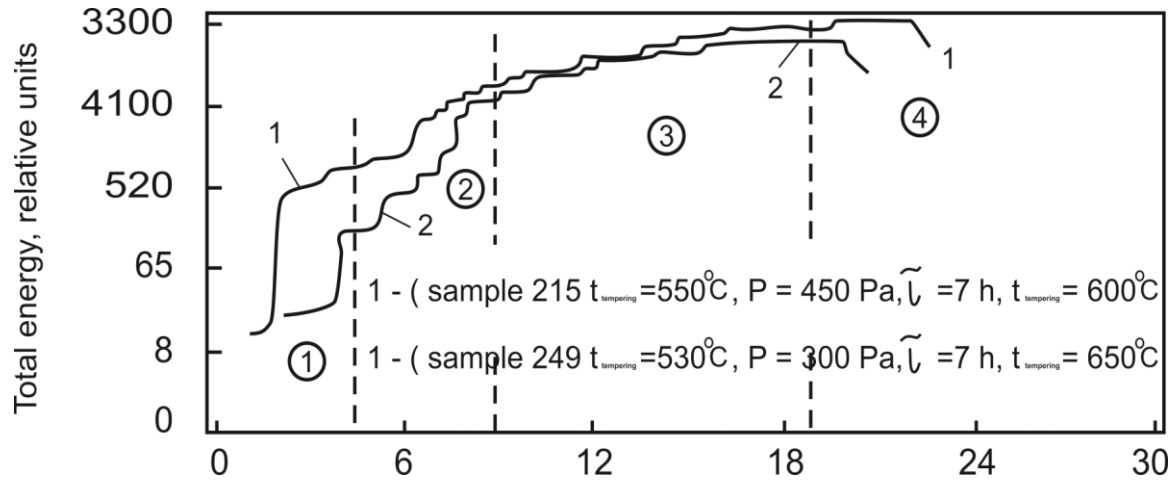

Figure 3. *Total energy change with respect to the load for the nitridd samples*

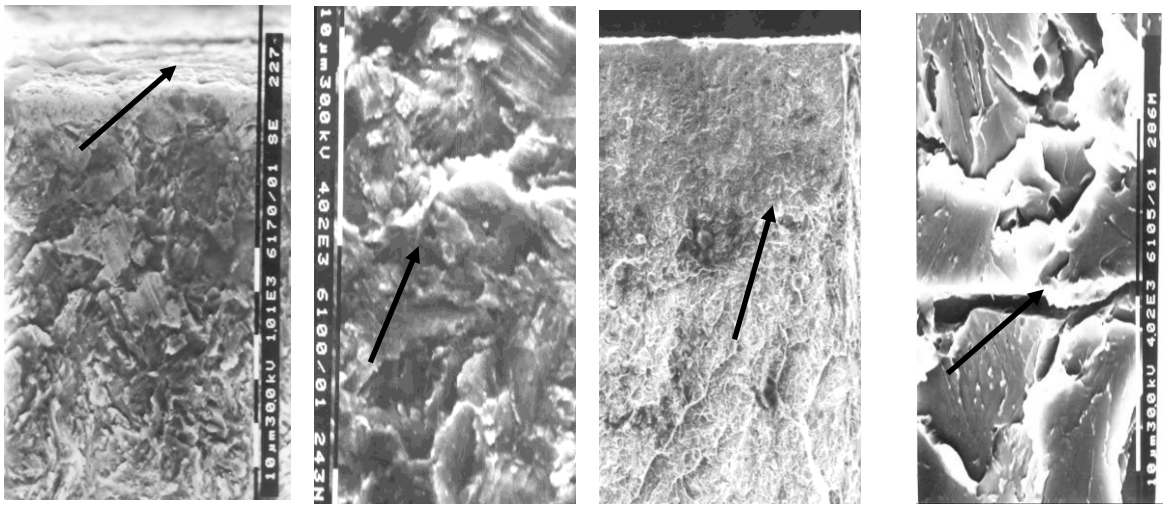

a b c d

Figure 4. *Fracto-graphs of the ion-nitrided samples*

This is due to the higher brittleness of the combined zone. For these loads the micro-deformations in the diffusion zone are sufficient for achieving the critical destructive stresses in the imperfect (defective) sections of the layer, primarily the areas with high density of dislocations around the nitride (carbonitride) depositions [1,12].

At these initial loads micro-cracks are not formed in the non-nitrided matrix, what is due to the lower modulus of elasticity and the arising (because of that) lower stresses in it at the same levels of deformation. On the other hand, the matrix is much more plastic than the nitrided layer.

Only at heavier loads plastic deformation occurs in front of the notch in the matrix – Fig. 2, ②. This causes microcracking of the biggest carbide particles, having the highest density, which are located in the plastic zone or in closest proximity to it, which leads to appearance of microcracks in the matrix as well [6,7,11,12]. The closest to the layer newly formed microcracks do not propagate in it, since the diffusion zone prevents from plastic deformation occurrence at these stresses. The propagation of the micro-cracks in the layer is also impeded by the residual compressive stresses and the higher hardness of the layer.

After certain level of loading, conditions arise for propagation of the formed micro-cracks both in the layer (combined zone and diffusion zone) and in the matrix. Some microcracks in the matrix and the layer move and merge to form a larger (magistral) crack, which propagates along the boundary between the diffusion zone and the matrix – Fig. 4c,d – most probably where the compressive stresses are very low or change their sign. The crack develops unsteadily after reaching the critical micro-stresses for initiating brittle fracture (Fig.2), zone ③. This magistral crack, located at the boundary between the layer and the matrix obviously has the greatest contribution to the process of splitting off the layer and fracture of the nitrided body. Naturally, the other cracks in the layer and the matrix also have their influence on this process. The nitrided layer breaks last - (Fig.2), zone ③.

IV. CONCLUSIONS

The acoustic emission can be used as an indicator of pre-fracture processes in nitrided details.

A probable mechanism of fracture of nitrided materials is proposed.

References

[1] Maksimovich, G, V. Shatynskij V. Kopilov, Pysical and chemical processes in plasma dusting and destruction of coated materials, Kiev, Naukova dumka, 1983, p.260

[2] Lozev, M., Application of the acoustic emission for non-destructive control of vessels, working under pressure, Mechanical Engineering, 11, 1984, pp.507-509 .

[3] Lozev M., A.Zyumbyulev, V.Toshkov and L.Boev, Fracture mechanics of ion-nitrided steel, Materials Science, Volume 28, Number 2, March ,1993, pp. 116-119

[4] Khan M. A., Shoji T., Takahashi B., Acoustic Emission from cleavage microcracking in alloy steels, Metals Science, Vol.16, 1982, pp= 118-126.

[5] Grunling H. W., Schneider K., Singheiser L., Mechanical Properties of Coated Systems, Materials Science and Engineering, 88, 1987, pp. 177-189.

[6] Okuno T., Effect of microstructure on the toughness of hot work tools, Steel AINI, H13, H10, H11, Transactions ISIY, Vol.27, 1987, pp.51-55.

[7] Qamar S., Sheikh A., Arif A., Pervez, Siddiqui R., Heat treatment of a hot work die steel, Archives of Materials Science and Engineering, Volume 28, Issue 8, August 2007, pp. 503-508.

[8] Toshkov V., A. Zumbilev and M. Lozev, On Some Aspects of the Fracture of Heat Treated and Ion Nitrided Steels, Proceedings of 5th International Seminar on "Heat Treatment and Surface Engineering"26-29, IX, 1995, Isfahan, Iran, pp. 265-270.

[9] BS 5447--1977 Methods of test for plane strain fracture toughness (K_{Ic}) of metallic materials.

[10] BS 5762-1979.Methods for crack opening displacement (COD) testing.

[11] Zumbilev A., About the influence of heat treatment over the resistance against fragile destruction of BH21 steel Technical university Journal "Annals of the faculty of engineering Hunedoara", Tome VIII, Fascicle 1 (ISSN1584/2665), Romania, 2010, pp.21-24.

[12] Zumbllev A., About the influence of the process of ion nitriding over the critical crack opening in BH21 steel. Journal "Annals of the Faculty of Engineering Hunedoara", Tome X, Fascicle 1, 2012, Romania, pp. 67-70.

[13] Acoustic emission in the diagnostics of pre-destructive state and forecasting destruction of welded constructions, Papers, International School, 1986, p.146 .

[14] Lozev M., Acoustic evaluation of austenitic welded joints, Chimmash, Informa, Sofia, 1990, p.44.

[15] Mihovski M., M. Lozev, Non-destructive control in chemical machine building, Techniques, 1987, p. 159 .

[16] Bunina, N., Studying plastic deformation of metals by the method of acoustic emission, Leningrad University, 1990, p. 156 .

RESEARCH OF DRYING OF BREWER PELLETS AIMED AT INCREASING OF ITS EFFICIENCY AND LOWERING OF POWER CONSUMPTION

Sukmanov Valerii[1], Bessarab Oleksandr[2], Shutyuk Vitaliy[2], Stefanov S[3]

1- *Higher Educational Institution of Ukoopspilka "Poltava University of Economics and Trade" (PUET), Poltava, Ukraine, e-mail: sukmanov53@mail.ru*
2- *[2] – National University of Food Technologies (NUFT), Kyiv, Ukraine*
3- *[3] – University of Food Technologies (UFT), Plovdiv, Bulgaria*

Abstract: *This paper presents the results of research of the drying process in the brewer pellets in aerovibrofluidized bed. The kinetics of drying of pellets in the suspension bed has been experimentally studied. We have received the generalized drying curve of brewer pellets at different process conditions. The generalized drying curve received as a collocation of the drying curves of brewer pellets at different process conditions is an indication of constant value of speed multiplied by time of drying, which simplifies the calculations of changes in moisture content during certain periods of the heat treatment of the product. We offered the relative ratio of energy consumption; proportionality factor of performance and bed depth; qualified expenditure power consumption indicator, which allow to reasonably choose conditions of brewer pellets drying and significantly improve the value of energy saving performance indicators of the drying process. There have also been introduced the parameters of qualified expenditure power consumption and the non-dimentional coefficient of power consumption.*

Keywords: drying, aerovibrofluidized bed, brewer pellets, energy efficiency

Introduce

One of the most energy-intensive processes in the food production process is the drying of raw materials and food products.

Breweries produce large quantities of various kinds of waste, the majority of which comprises osier pellets. This «byproduct» in its raw state is widely used by stock-breeders as a high-energy protein supplement for animal feeding stuff. In winter the problem of selling raw brewer pellets is virtually absent, but in summer farmers prefer to use green fodder. Meanwhile in the breweries accumulates a large amount of waste, the term of storage of which is limited to several tens of hours due to the rapid fermentation and mold formation.

Brewing waste is now often considered as a source of raw material with high nutritional value and biological activity used for feeding livestock and poultry. A medium power brewery annually produces 35,000 tons of brewer pellets which go to waste, and effective methods of preservation of the product (except for drying) do not exist. Drying of pellets is not used due to lack of energy-saving equipment [1, 2]. Such issues as large-tonnage waste recycling of brewer pellets should also be tackled because many factories pour them down the drain, causing the worsening of environmental situation in Ukraine.

Dry brewer pellets are widely used in meat, bread-baking and other food industries. Drying of brewery pellets to a final moisture content of 10% results in a long term of storage, which makes production and transportation over long distances cost-effective. The solid residue can be used for a whole range of valuable products, since it contains about 8 % of lipids, 26 % of proteins, 58 % of carbohydrates, as well as minerals, vitamins and other biologically active substances [3, 4].

Unfortunately, the existing drying processes of brewer pellets are extremely energy-consuming. Having modern technologies of thermal processing of high-materials (pellets contain more than 80 % of moisture) and at the same time imperfect technical equipment, it is necessary to develop advanced high-tech and low-power processes of brewer pellets and create equipment on the basis of new developments in the field of drying.

The most intensive process is the convective heat and mass transfer between the continuous gas medium and solid particles dispersed in a vibrofluidized pseudoliquified bed.

Vibrofluidized bed is formed either under the influence of vibrations only, or as a result of combined effect of vibrations and air movement. During the drying in the vibrofluidized bed particulate material may be brought into pseudoliquified condition due to the influence of

vibrations on it. Vibratory oscillations of the working surface (grid) with a frequency of 40…60 Hz and an amplitude of 2…10 mm are generated by mechanical, hydraulic, electromagnetic vibrators. Shaking drier is successfully used for dewatering particulates prone to adhesion, which reduces energy costs compared to the cost of the material in the recycling or loading of wet material on a layer of a dry one. In this case, the speed of air is lower, the losses due to moisture pickup also decrease [5, 6].

The analysis of existing information on the subject suggests that the degree of influence of heat on heat labile components is primarily a function of temperature and duration of the thermal interference, as well as pH, amount of enzymes and other factors. Thus, the criterion for the heat resistance of products may be the maximum allowable temperature of heating in the drying process [7, 8].

Food drying in the pseudoliquified (aerovibrofluidized) bed is a common process, but it is understudied and has not been used for preserving brewer pellets [9].

The aim of the paper is research and development of the process of brewer pellets drying in a vibrofluidized bed, characterized by high energy efficiency.

Methodology of research and materials

The drying of pellets in the experimental assembly was carried out at the following values of parameters: temperature of the drying agent (air) – 50…70^{0}C; lattice vibrations: frequency F = 2…50 Hz, the amplitude A = 2…10 mm; air velocity – 0,5…3,0 m/s.

Such an upper limit of the drying temperature was chosen because at higher temperatures the proteins turn into unpalatable form, the pellets darken due to caramelization and formation of melanoids, part of the vitamins gets destroyed. At a temperature of less than 50°C, the drying process slows down, energy consumption increases.

To achieve the objectives we have developed the design of the experimental setup for drying of brewer pellets (Fig. 1 – the general view of the stand and Fig. 2 – the diagram of an experimental assembly), which is equipped with thermal, mechanical, control, measurement devices and registering apparatus [10, 11].

To investigate the brewer pellets drying parameters we have configured the measuring system (Fig. 3), which works in conjunction with a computer. A multi-channel system is intended for solving the tasks connected with the collection, processing, storage, visual display of information gathered both in real time and after summing up the measurements.

The measuring system consists of normalizers, commutators, analog-to-digital, digital-to-analog converters and software. There were used chromel-copel thermocouple sensors with point and differential measurements of process parameters.

Fig. 1. General view of the stand for experimental research of brewer pellets drier
1 – cyclone; 2 – exhaust fan; 3 – drying chamber; 4 – vibrator; 5 – sensors of drying parameters; 6 – regulators of power supply; 7 – the pressure fan; 8 – electric heater; 9 – sensor signal converter; 10 – measuring unit.

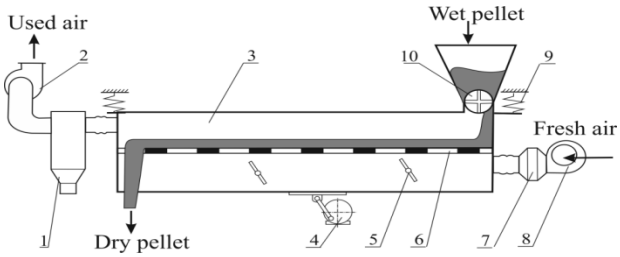

Fig. 2. The diagram of experimental drier of brewer pellets
1 – centrifugal collector; 2 – exhaust fan; 3 – drying chamber; 4 – vibrator; 5 – rotary plate; 6 – perforated screen; 7 – heater; 8 – the pressure fan; 9 – spring suspension; 10 – feeder unit.

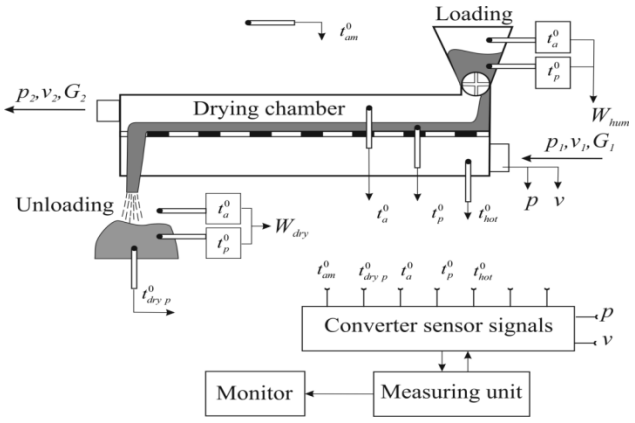

Fig. 3. Measuring diagram of the experimental dryer

t_{am} – ambient temperature; t_{hot} – hot air temperature; $t_{dry\ p}$ – the temperature of the dry product; t_a – ambient temperature above the product; t_p – the temperature in the layer of the product; W_{hum} – humidity of the raw pellets; W_{dry} – moisture of dry pellets; p – pressure of hot air; v – velocity of hot air.

The moisture of the pellets was determined in accordance with the instructions of technical-chemical control of the brewing industry in the «Sarmat» laboratory of the brewery. A portion of 8…10 g of raw pellet was placed in a weighing bottle and dried for 2 hours at a temperature of 60^0C and for 3 hours at a temperature of 105^0C. Calculation of moisture was carried out with the help of the formula

$$W = [(a - b)/(a - c)]\cdot 100, \quad (1)$$

where, a – is weight of the weighing bottle with the sample before drying, g; b – weight of weighing bottle with the sample after drying, g; c – weight of the empty weighing bottle, g.

Ambient humidity was measured with a hygrometer.

The temperature was measured with chromel-copel thermocouples located: t_{am} – in the environment; t_a – over the brewer pellets in the hopper and in the workroom; t_p – in the layer of the product; t_{hot} – under the layer of the product; $t_{dry\ p}$ – in a dry product with an output to analog recorder.

Measurement of the air flow rate and volumetric flow rate was done using hot-wire anemometer *Testo 415*, which allows to simultaneously measure air velocity and the temperature of it, which enabled us to confirm the readings of thermocouples. Measurements were made under the grid at the inlet to the operating chamber and at the outlet from the operating chamber. The magnitude of the hot air pressure was measured by changing the voltage supplied to the pressure fan.

The frequency of vibration was adjusted with a mechanical tachometer Testo 470. The density of the brewed pellets at various stages of the drying process was determined by weighing 0,001 m^3 of the substance. Regulation of the amplitude in the range of 1 to 10 mm was performed by moving the connecting rod pin in the direction from the center of rotation of the motor shaft. Supply air temperature control was carried out by changing the voltage supplied to the heater.

Before the start of the experiment the moisture of pellets was measured, and then the pellets had to undergo further drying. The tilt angle of the drying chamber which determines the speed of transportation of the drying product equals $8…10^0$.

Brewer pellets, previously pressed resulting in a moisture content of 70…80%, were loaded into the receiving hopper of the experimental assembly. Due to the fact that the length of the experimental assembly (1000 mm) is not sufficient to completely dry the product, the batch of brewer pellets after each cycle was loaded again into the working chamber and the cycle repeated. Every 4 minutes samples were taken to determine the moisture content. The total drying time was about 1600 s.

III. Results and discussion

3.1. Investigation of the process of pseudoliquifying of the pellets.

Analysis of priori information on the application of complex effect on the dried product of coolant and vibration allowed to focus on the defining of such values as the flow rate of the coolant, the frequency and amplitude of the vibrations of the supporting sieve, the initial height of the filling layer, the influence of which on the hydrodynamics of the brewer pellets drying process is understudied.

Since the horizontal transfer of particles is predetermined by passing through layer of gas bubbles, the model of horizontal mixing should be presented as the diffusion of solid particles in a turbulent flow in a three-dimensional random velocity field and described as a random Markov process [12].

It has been found that the rate of upward flow of air should be sufficient to overcome the gravitational forces of filling of material particles, therefore, the most significant characteristic of the pseudoliquifying process is the value of air velocity.

Graphic relationship between hydraulic resistance Δp (pressure drop) of the product layer and the speed of the fluidizing air v_f in an unfilled section of the drying chamber was drawn according to experimental data. To receive these data, we used two U-shaped manometers, indicating pressure «under» and «above» the layer of brewer pellets. The rate corresponding to the inflection on the curves (Fig. 4) equal 2,0 m/s we shall call the velocity in beginning of pseudofluidization v_{f1} or the first critical pseudofluidization velocity. Starting with the velocity v_{f1} the value of Δp with increasing v_f almost does not rise. Upon reaching the second critical velocity of air v_{f2} begins the carry-over of a layer of the product even if it is underdried. Figure 4 shows a decrease in the value of Δp at $v_f > v_{f2}$, due to diminution of the material in the layer due to the carry-over of the individual particles.

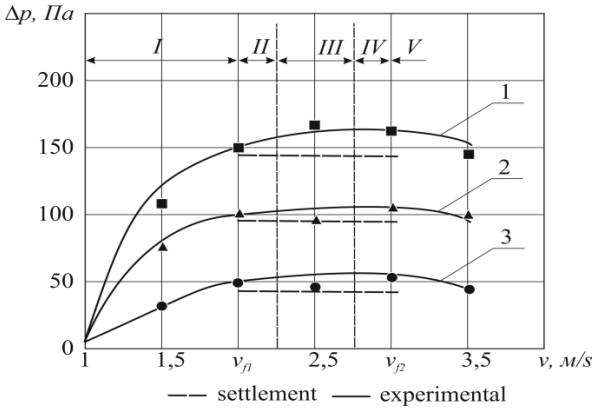

Fig. 4. Curves of pseudofluidization of brewer pellets at different heights of filling
1 – filling height is 20 mm; 2 – filling height is 30 mm; 3 – filling height is 40 mm

Analysis of the curves shows that the value of v_f is independent of the height of fluidizing layer of the product. The height of the layer determines only a resistance value Δp of the air flow passing through this layer. The calculated rate appeared to be a bit underestimated compared to experimental one due to averaging in calculating the load factor Δp.

In industrial dryer operation pseudofluidization velocity of the brewer pellets v_{op}, including scaling is 3…10 times greater than the starting velocity of fluidization v_{f1}. Therefore, in practical calculations, one can use the equation [6], which determines the ratio of the velocity of pseudofluidization

$$K_v = v_{op}/v_{f1}. \quad (2)$$

For experimental brewer pellets dryer the range of numbers of pseudofluidization $K_{v,}$ in which there may be included a fluidized bed, the velocity is determined by the ratio of carry-over v_{n2} and the start of pseudofluidization v_{f1}, i. e., $K = v_{f2}/v_{f1} = 3/2 = 1{,}5$. Liquefaction stage in Figure 4 are marked with the fields: *I* – the beginning of the disintegration of the layer; *II* – channel incrush of air; *III* – the destruction of channels and boiling, *IV* – active swirling boiling, *V* – carry-over. With an increase of fluidization occurs intensification of movement of the particles in the layer resulting in increase of its porosity, defined by the formula

$$\varepsilon = V_{air}/(V_{air} + V_{pel}), \quad (3)$$

where V_{air} – volume of air between the particles of the pellets; V_{pel} - the volume occupied by the pellets' particles.

The average value of porosity of unliquefied pellets is 0,6…0,7. During liquefaction – ε = 0,8…0,9, and under carry-over conditions ε equals one, since in this case the volume of air between the particles of pellet is much larger than volume occupied by the particles themselves.

The height of the pellets layer (filling) has been calculated experimentally, according to the well-known statement on the lower energy consumption at the lower layers, taking up more space than in the case of high layers on smaller areas. The loaded on the sieve layers of pellets from 10 mm to 60 mm were examined, and we found the following:

– at a height of layer of 10 mm drying rate is relatively high, but there is a danger of carry-over of underdried particles; at a layer height of 50…60 mm there is no constant drying rate and the process is significantly delayed in time; best results are obtained when loading the layer of 30 mm, when there were two periods of drying - the periods of constant and decreasing velocities.

3.2. Investigation of the kinetics of pellets drying in a suspension bed.

The main characteristics of the drying process of brewer pellets are kinetic functional connections between the product moisture changes and the duration of the process, the rate of change of humidity, pattern of temperature change of the material during the drying process under certain environmental conditions.

On the basis of the available information on the collocation and linearization of curves of drying [6], in order to reduce the number of experiments we conducted fractional factorial experiment that implements part (fractional replica) of the full factorial experiment of the 2^{4-1} type. The plan is assigned by generating relation $x_4=x_1x_2x_3$. Defining contrast is the relation $1 = x_1x_2x_3x_4$. Concurrently, the regression equation is of the form

$$y = b_0 + b_1x_1 + \ldots + b_px_p. \quad (4)$$

where y – the outputs vector – moisture of the brewer pellets; x_1, x_2, x_3, x_4 – vectors of the input parameters: x_1 – the temperature of the drying medium (air); x_2 – the sieve load (bed height of the product); x_3 - the speed of the drying agent; x_4 - parameters of the sieve vibration (frequency and amplitude).

The plan was executed by stepwise defining of the output value. At the same time were taken levels of varying input parameters, the reason for choosing which was mentioned above (Table 1).

Table 1

Parameters of the investigated process

Parameter	Symbol and unit	The lower level	The upper level
x_1	t, ^{0}C	50	70
x_2	h_0, mm	20	40

x_3	v, m/s	2,5	3,5
x_4	F/A, Hz/mm	10/10	17/4

Step 1: $y^{(1)} = f(\tau)$ at x_1 = 50^{0}C; 60^{0}C; 70^{0}C; x_2, x_3,x_4 = const.

Step 2: $y^{(2)} = f(\tau)$ at x_2 =20; 30; 40 mm; x_1, x_3, x_4 = const.

Step 3: $y^{(3)} = f(\tau)$ at x_3 =2,5; 3,0; 3,5 m/s; x_1, x_2, x_4 = const.

Step 4: $y^{(4)} = f(\tau)$ at x_4 =10/10; 13,5/7; 17/4 Hz/mm; x_1, x_2, x_3 = const.

On the basis of experimental pellet drying in order to receive constant weight under conditions of triplicate experiments and overlapping of their results within the measurement accuracy we plotted charts of drying and drying rate at the varying temperature of the drying agent, the sieve loads (of the initial bed height), speed of drying agent and the vibration parameters, the values of which are given in Table 1.

Stage 1. Experimental drying was carried out at three different temperature values of a drying agent (air) t: 50, 60 and 70^{0}C. In each of three experiments bed height h_0 = 30 mm, the speed of the drying agent v = 2,5 m/s, the parameters of the sieve vibration (frequency F = 13,5 Hz and the vibration amplitude A = 7 mm) remained constant. As the drying agent we used air with temperature of 50, 60, 70^{0}C and relative humidity of 30%. Initial moisture W^{raw} of the raw pellets was 400%, the final equilibrium water content – 9…10%.

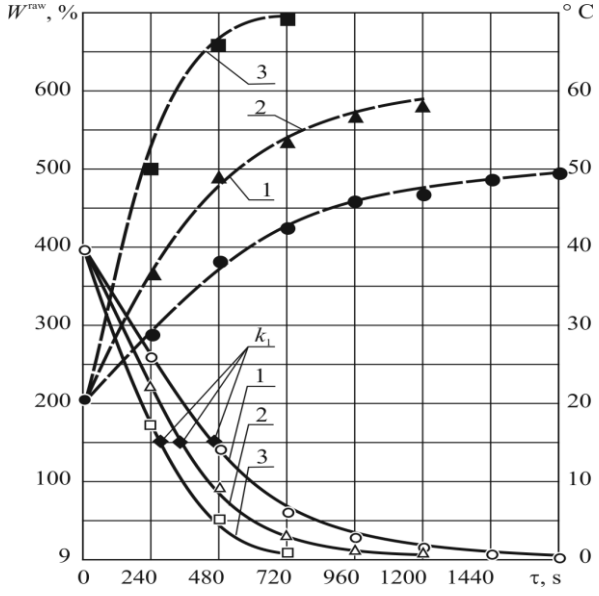

Fig. 5. Curves of changes in moisture content and temperature during the drying of brewer pellets at varying temperature of the drying agent

1 – at the temperature of the drying agent t = 50^{0}C; 2 – at t = 60^{0}C; 3 – at t =70^{0}C. The initial layer height of the product h = 30 mm; speed of the drying agent υ = 3,0 m/s; vibration parameters: F = 13,5 Hz, A = 7 mm.

Figure 5 shows graphical relations of the kinetics of humidity changes during the drying of brewer pellets $W^{raw} = f(\tau)$, obtained after processing the results of measurements of moisture loss given in the table.

Curves have a straight section from the beginning of drying to the point k_1. In this period, the drying process takes place at a constant speed and is identical to the process of evaporation of the liquid from the free surface, thus, on the basis of the Dalton's law it can be described by the expression:

$$-\frac{dW}{d\tau} = A(1-\phi_0)\exp\left(-\frac{A\rho_0 h_0}{\upsilon\rho_{dry\,a}100}\right), \quad (6)$$

where W is moisture content, %; τ – time, s; A - coefficient characterizing the mass transfer; φ – the initial relative humidity of the drying agent, %; ρ_0 and $\rho_{dry\,a.}$ – the density of freely poured layer of material and drying agent respectively, kg/m^3; h_0 – initial height of the freely poured (dense) layer of material, m; v – speed of the drying agent, m/s.

The nature of the changes in moisture content suggests that the drying of the brewer pellets significantly depends on the temperature of the drying agent. When the air temperature equals 50^{0}C (curve 1 in Fig. 5), the duration of the dewatering in the second period (at falling speed) is 2.5 times the duration of the dewatering in the first period (constant speed); with an air temperature of 60^{0}C (curve 2 in Fig. 5) the ratio of the periods remains constant, but the overall drying duration at this temperature is reduced by 1.4 times; increasing the air temperature to 70^{0}C (curve 3 in Fig. 5) results in a decrease in the total duration of the process in 2,3 times as compared with the first temperature control. More than half of the moisture contained in the product evaporates in the first period of drying, regardless of temperature. Analyzing all written above, it can be noted that in the first case the process is delayed in time and does not provide optimum performance of the process vessel and in case of temperature increase of the drying agent to 70^{0}C there is a risk of failing to preserve the quality of the final product.

The analysis of temperature curves shows that the increase in temperature of the brewer pellets at the constant speed of drying passes rapidly. Later the temperature continues to increase, but its rate of

growth slows down and stabilizes at approximately the equilibrium water content when drying process is considered complete. At this time, the temperature inside the product layer differs from the temperature of the hot air by several degrees (2…3^{0}C).

Step 2. Experimental drying was carried out at different initial bed height of the product: h_0 = 20 mm; h_0 = 30 mm; h_0 = 40 mm. In each of the experiments temperature of the drying agent t = 60^{0}C, rate of drying agent v = 3,0 m/s, the vibration parameters of the sieve F = 13,5 Hz and A = 7 mm remained constant. The parameters of the drying agent, the initial and the equilibrium moisture content of pellet are the same as in the first step.

Graphic processing of the experimental results is displayed in Figure 6 in the form of curves which show relation $W = f(\tau)$.

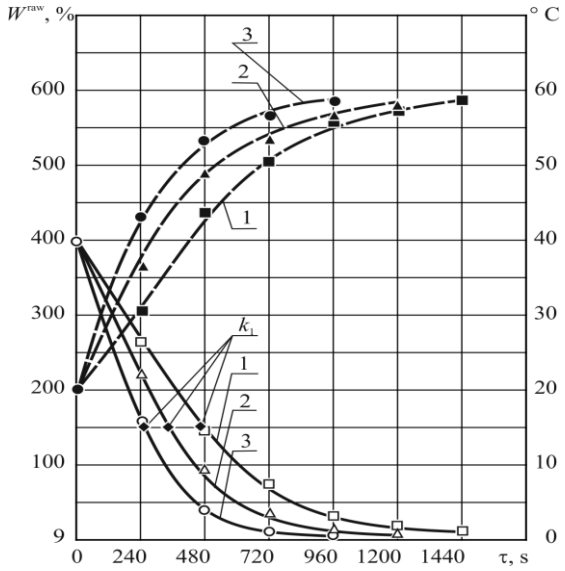

Fig. 6. Curves of changes in moisture content and temperature during the drying of brewer pellets at varying load (bed height)
1 – the initial bed height h_0 = 20 mm; 2 – at h_0 = 30 mm; 3 – at h_0 = 40 mm.
The temperature of the drying medium t = 60^{0}C; speed of the drying agent v = 3,0 m/s; vibration parameters: F = 13,5 Hz; A = 7 mm.

The curves in Figure 6 display an increase in the duration of the process by increasing the thickness of the product layer from 20 mm (curve 1) to 40 mm (curve 3). In the observed case, the total drying time increased by 1,5 times due to the slow evaporation of water in the second period. At the same time a high rate of dehydration in the first period of drying is maintained, which corresponds and is explained with the help of the components of the expression (4). The heating rate of the product varies, as indicated by the rapid rise in temperature in the first stage of drying (up to critical moisture content) and flattening of the curves in the second period. However, a noticeable effect of the thickness of the product layer on the drying time is less noticeable than the effect of the temperature of drying agent, as shown above (Fig. 5). By the end of the drying curves get closer and final drying is carried out in the same way at decreasing speed.

Stage 3. Experimental research on drying of brewer pellets was carried out at three different values of speed of the drying agent, constant parameters given in the picture captions (Fig. 7), the initial moisture content W^{mc} = 400%, the equilibrium moisture content W^{mc}_{eq} = 9...10%. As a drying agent we used ambient air with an initial temperature of 20 °C and relative humidity of 30%.

Comparison of curves 1 and 2 (Fig. 7) in the moment of reaching the equilibrium moisture content of the product shows that the increase in the speed of the drying agent from 2,5 to 3,5 m/s shortens the duration of the drying process by 67%. Thereby, the duration of the first drying period, when evaporates more than a half of the water contained in the brewer pellets, is affected by the change of speed of the drying agent less (20%) than by the change in temperature of a drying agent (Fig. 5) and the change in the height of the layer (Fig. 6). Temperature curves in this experiment are very close to each other, particularly in the second period, displaying the fact that the process takes place at relatively high and, consequently, energy-consuming, temperatures.

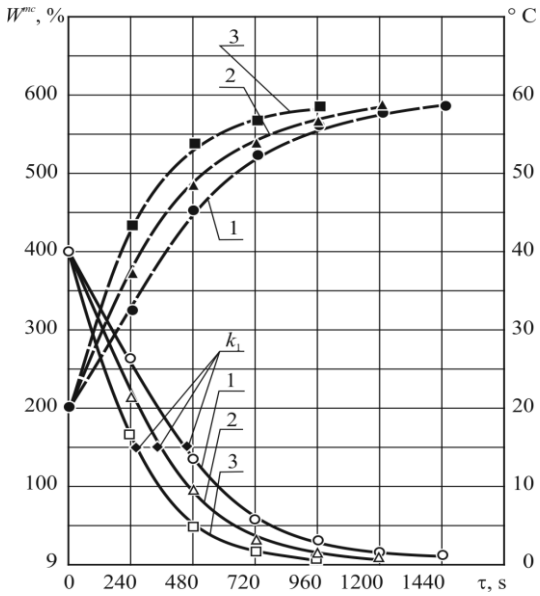

Fig. 7. Curves of change in moisture content and temperature during drying process of brewer pellets at varying speed of the drying agent

1 – at the speed of the drying agent v = 2,5 m/s; 2 – at v = 3,0 m/s; 3 – at v = 3,5 m/s.
The temperature of the drying medium $t = 60^0$C; the product's initial height h = 30 mm; vibration parameters: F = 13,5 Hz, A = 7 mm.

Step 4. We have investigated the batches of brewer pellets with free filling bed height h = 30 mm, the initial moisture content of 400%, which were blown by the hot air at $t = 60^0$C and velocity v = 3,0 m/s. A sieve with a product was cited in the vertical oscillation at a frequency of 10; 13,5; 17 Hz and an amplitude of 10, 7, 4 mm. The range and oscillation parameters were defined in a preliminary test of the drier with a product load and were taken by us as the most efficient from a wide range of parameters recommended by the authors [5, 13].

Drying curves 1, 2, 3 (Fig. 8) plotted within the range of change of vibration parameters display a slight (16%), reduction of the drying time in the transition from a relatively high frequency of 17 Hz to a lower frequency – 10 Hz. Frequencies of 10 and 13,5 Hz almost identically influence the duration of the process (curves 1 and 2), while the oscillation frequency equal or close to 17 Hz (curve 3) can be considered less effective.

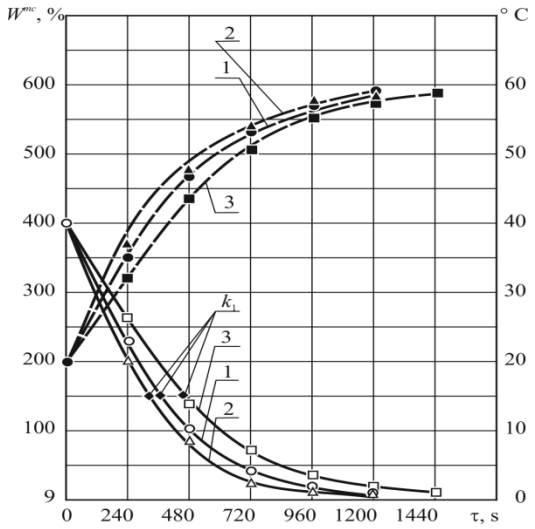

Fig. 8. Curves of change in moisture content and temperature during the drying of brewer pellets at varying parameters of sieve vibration
1 – at the oscillation frequency of the sieve F = 10 Hz and the amplitude A = 10 mm; 2 - at F = 13,5 Hz and A = 7 mm; 3 - at F = 17 Hz and A = 4 mm.
The temperature of the drying medium $t = 60^0$C; The product's initial height h = 30 mm; the speed of the drying agent υ = 3,0 m/s.

At the same time, the determining factor of occurrence of aerovibrofluidized bed, along with the speed of the air, is sieve vibration and the fact that all the previous results (steps 1, 2, 3) were obtained using motion parameters corresponding to the selected range. Therefore, curves 1 and 2 indicated the correct selection of the oscillation frequency F = 13,5 Hz and the amplitude A = 7 mm.

Comparing the results of the research, we made a conclusion about a significant impact on the drying temperature of the drying agent (Fig. 5) and the bed height of the product (Fig. 6). Less effective factors are the speed of the drying agent (Fig. 7) and the parameters of sieve vibration (Fig. 8). The latter is explained by the small range of permissible values of the factors mentioned.

The empirical formulae describing the change in moisture content of brewer pellets (Figure 5–8), were obtained with the help of the software «Curve Expert 1.3» and presented in the following form:

$Y = a + bx + cx^2 + dx^3$ – for the curves 1 and 2;

$y = a \cdot exp(-(b - x)^2/2c^2$ – for the curve 3

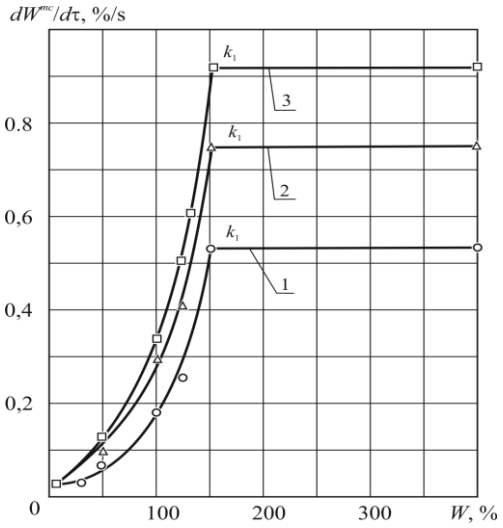

Fig. 9. Curves of drying speed of the brewer pellets obtained by graphical differentiation
1 – at the temperature of the drying agent $t = 50^0$C; 2 – at $t = 60^0$C; 3 – at $t = 70^0$C.
The initial product layer height h = 30 mm; speed of the drying agent υ = 3,0 m/s; vibration parameters: F = 13,5 Hz, A = 7 mm.

In order to further analyze the kinetics of drying grains we carried out graphical differentiation of curves of drying and plotted the charts of drying speed $dW^{mc}/d\tau = f(W)$ (Fig. 9).

Curves 1, 2, 3 (Fig. 9) during the process of drying the pellets in a pseudofluidized state have horizontal sections of the fixed speed corresponding

to intensive drying, and slanting curves which indicate the falling speed. It is evident that higher temperatures of the drying agent correspond to the higher drying rate in the first period of the process. When reaching the critical point K_1, the speed begins to fall, and all the curves come closer and asymptotically approach the value of the equilibrium state. This drop can be explained by the reduction of the moisture content on the surface and an increasing of internal resistance of the heat transfer. Curves of speed of pellets drying of the second stage of research (varying of the bed height of the product) do not differ from the process intensity of the ones given above. A thinner layer of product dries more quickly.

To calculate the root-mean-square error of the measurements and determine whether the experimental distribution corresponds to the normal distribution law we used a graphical method of processing the results by comparing the experimental distribution curves with a set of theoretical curves. The root-mean-square deviation did not exceed 9,3%.

3.3. Determination of the process parameters on the basis of experimental data.

On the basis of the experimental brewer pellet drying to constant weight under condition of triplicate experiments and overlapping of their results within the measurement accuracy curves of drying and the rate of the product drying were obtained at varying temperatures of the drying agent (air), the sieve load (bed height), air speed and vibration parameters. When comparing the results of studies we have suggested that the most significant impact on the drying has air temperature (Fig. 5) and the bed height of the product (Fig. 6), while the influence of parameters reflected in the curves in Figures 7 and 8 are less important.

Combining the curves of drying of brewer pellets obtained in these modes, in a generalized curve (Fig. 10) by the method of V. Krasnikova [6] proves that he product of speed and drying time $N\tau$ is constant and simplifies calculations of changes in moisture content both in the first and second period of heat treatment of the product.

Analysis of the generalized curve characterizing the kinetics of drying of pellets displays that the experimental points lie practically on the same curve, plotted in coordinates $W^{mc} - W^{mc}_{eq} = f(N\tau)$.

The curves received allow to determine the drying time and the current moisture content of the product, but not to select an efficient mode, since there is no criterion for selection. Having included in the search of such a mode the values of performance and power consumption, we made a comparison of the experimental data on drying of pellets at different modes (Table 2).

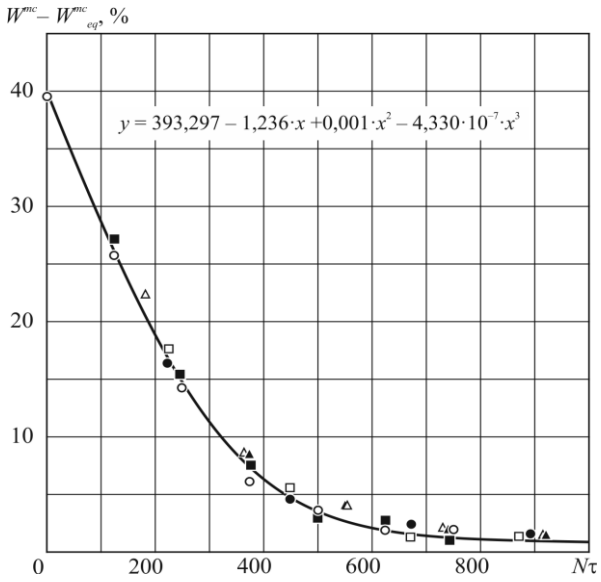

Fig. 10. The generalized curve of drying of the brewer pellets at various modes of drying

Mode 1. The temperature of the drying agent *t:* ○ – 50^0C; Δ – 60^0C; □ – 70^0C.
The initial height of the layer of product filling h_0 = 30 mm; speed of the drying agent v = 3,0 m/s; vibration parameters: F = 13,5 Hz, A = 7 mm.
Mode 2. The initial height of the layer h_0: ● – 20 мм; ▲ – 30 мм; ■ – 40 мм.
The temperature of the drying agent t =60^0C; speed of the drying agent v = 3,0 m/s; vibration parameters: F = 13,5 Hz, A = 7 mm.

Table 2

Comparison of experimental data on drying of brewer pellets at different modes

Pos.	Mode (fig. 3.11, 3.12)	Parameters of drying modes				Speed of drying, N	Duration of the 1st period, τ_1, h
		t, °C	h_0, mm	v, m/s	F/A, Hz/mm		
1	2	3	4	5	6	7	8
1	Mode 1.1	50	30	3,0	13,5/7	0,52	0,13
2	Mode 1.2	60	30	3,0	13,5/7	0,76	0,09
3	Mode 1.3	70	30	3,0	13,5/7	0,93	0,07
4	Mode 2.1	60	20	3,0	13,5/7	0,93	0,07
5	Mode 2.2	60	30	3,0	13,5/7	0,76	0,09
6	Mode 2.3	60	40	3,0	13,5/7	0,52	0,13

Continuation of the table 2

Duration of the 2nd period, τ_2, h	The total drying time, τ, h	Relation coefficient of energy consumption, K_{en}	Proportionality factor of performance and the layer height, K_p , 1/h	Qualified expenditure of electrical power ($\tau \cdot K_{en} \cdot K_p$), c.e.u.
9	10	11	12	13
0,33	0,46	1,00	30	13,8
0,24	0,33	1,23	30	12,2
0,13	0,20	1,50	30	9,0
0,20	0,27	1,23	20	6,6
0,24	0,33	1,23	30	12,2
0,27	0,40	1,23	40	19,7

Table 2 shows the nondimensional factor of energy K_{en}, which is defined as follows: the smallest defined capacity of electric equipment of the test bed according to one of the modes of drying is assigned with value equal to one. The coefficients of other modes were calculated on the basis of proportional relations of capacities.

Comparative analysis of the data in Table 2 is not the unambiguous definition of rational mode. In such way, if we choose energy consumption as the criterion for selecting the drying mode, the most economical would be considered the mode 2.1, at which conventional energy consumption is 6,6 c.e.u. (conventional electrical unit), and the drying rate – N = 0,93. However, the performance of the dryer is 1,5…2 times lower than in other modes under research. Low power consumption, high speed of drying, and the average value of the performance characterize the mode 1,3. Under industrial conditions, the temperature of the drying agent t can exceed 70^0C, when irreversible micro-processes on the surface of the product begin, leading to a rapid qualitative change in the structure of the product, which, in turn, prevents the intensity of water abstraction in the first period of drying. Modes 2.3 and 1.1 are the most energy consuming and prolonged in time ones, the drying process proceeds slowly at the speed N = 0,52, and hence, is characterized by low equipment performance.

On the basis of an examination of the modes it should be concluded that it is appropriate to conduct the process of drying of the pellets in the mode 1.2 at the air temperature t = 60^0C and conventional energy consumption of 12,2 c.e.u. At that the main criterion of the mode choosing is not the minimum power consumption, not a minimum drying time in general, but time, ensuring the preservation of high quality finished product [14].

IV. Conclusion

The experimental curves of changes in moisture content and temperature of the brewer pellets during the drying process at varying parameters of sieve vibration, layer height of the brewer pellets and speed of the drying agent, as well as the plotted generalized drying curve of the brewer pellets at various process modes and collocation of curves obtained at different modes in a single generalized

curve indicated that the product of speed and drying time is constant, which simplifies calculations of changes in moisture content during certain periods of the heat treatment of the product.

We have offered the relative ratio of energy consumption; proportionality factor on performance and the layer height; conditional energy consumption indicator, which allow to reasonably choose rational modes of drying of brewer pellets.

Reference

[1] Дегтерев С.В. Комплексная переработка отходов органического происхождения / С.В. Дегтерев, В.А. Горшков // Проблемы химии и экологии: тезисы докладов областной конференции молодых ученых и студентов / Пермский государственный комитет по охране окружающей среды. - Пермь, 2000. – С. 34.

[2] Пехер К. Тепловая утилизации пивной дробины — экономически выгодное использование экологически чистого источника энергии // Пиво и напитки. - 2006. - № 5. – С. 64-65.

[3] Дробот В.И. Использование нетрадиционного сырья в хлебопекарной промышленности: справочник / В.И. Дробот. – К.: Урожай, 2000. – 152 с.

[4] Использование пивной дробины при производстве колбасных изделий и полуфабрикатов / А. И. Сницарь, С. А. Рыжов, Е. М. Траханова, О. А. Маслобоев // Хранение и переработка сельхозсырья. - 2001. - № 10. - С. 59-60.

[5] Анатазевич В. И. Сушка пищевых продуктов: справочное пособие / В. И. Анатазевич. - М.: ДеЛи, 2000. - 296 с.

[6] Гинзбург А. С. Основы теории и техники сушки пищевых продуктов / А. С. Гинзбург. - М. : Пищ. пром-сть, 1973. - 528 с.

[7] Харченков К. В. Повышение эффективности рекуператоров тепла для сушилок солода К. В. Харченков // Пиво и напитки. - 2003. - № 3. - С. 18-19.

[8] Антипов С. Т.Технологическое оборудование для сушки пищевых продуктов / С. Т. Антипов. - М. : Агропромиздат, 1989. - 81 с.

[9] Сушіння пивної дробини для використання її в харчових технологіях / Г. І. Русланов, В. О. Сукманов, Н. М. Лавріненко, О. В. Гура // Харчові добавки. Харчування здорової та хворої людини: матеріали другої міжгалузевої міжнародної науково-практичної конференції, 5-7 квітня 2007 р. / Донецький національний університетт економіки і торгівлі ім. М. Туган-Барановського. – Донецьк, 2007. - С. 304-306.

[10] Пат. 9711, Україна, МПК A 23 L3/20, A 23 L3/16. Пристрій для сушіння пивної дробини / С. А Мельник, Г. І. Русланов, В. О. Сукманов, В. А. Хомічук, Н. М. Лавріненко ; заявник и патентовласник Донец. держ. ун-т економіки і торгівлі ім. М. Туган-Барановського. - № 20050002414, 20050317, заявл. 17.03.05 , надрук. 17.10.05, Бюл. № 10. – 2 с.

[11] Пат. 9712 Україна, МПК A 23 B 7/028, B 02 C 4/00, A 23 B 7/02. Спосіб сушіння високовологих продуктів / С. А. Мельник, Г. І. Русланов, В. О. Сукманов, В. А. Хомічук, Н. М. Лавріненко ; заявник и патентовласник Донец. держ. ун-т економіки і торгівлі ім. М. Туган-Барановського. - № 20050317, заявл. 17.03.05 , опубл. 17.10.05, Бюл. № 10. – 2 с.

[12] Лавріненко Н. М. Моделювання процесу дифузії твердих частинок у псевдо зрідженому шарі / Н. М. Лавріненко, О. В. Гура // Зб. наук. праць / Одеська держ. акад. холод. техники. – О., 2006. – Вип. 28, т. 2. – С. 223-225.

[13] Оптимальный режим сушки на основе математического моделирования / Хараев Г. И., Котова Т. И., Комиссаров Ю. А., Хантургаева Г. И. // Хранение и переработка сельхозсырья. – 2007. - № 9. - С. 28-30.

[14] Пат. 18742, Украина, МПК A 23 L 3/16; A 23 L 3/16. Пристрій для сушіння пивної дробини на вібруючий поверхні / О. В. Гура, Г. І. Русланов, В. О. Сукманов, Н. М. Лавріненко ; заявник и патентовласник Донец. держ. ун-т економіки і торгівлі ім. М. Туган-Барановського. - № 18742, опубл. 15.11.2006, Бюл. № 11. - 3 с.

Experimental study on mechanical properties of NBR-based rubber mixture

Delyan Gospodinov[1], Vilhelm Hadjiski[1], Donka DONEVA[2]

[1] *University for food technologies – Plovdiv, Plovdiv, Bulgaria, dgosp@abv.bg*

[2] *ZKU Stara Zagora, Gorno Botevo, municipality of Stara Zagora, Bulgaria*

Abstract. *An experimental study has been conducted to determine some mechanical properties of NBR-based vulcanized rubber compound which is used for the production of O-shaped ring gaskets which are very common in the technological equipments used in the food-processing industry. The effects of the ageing process of the rubber on the parameters in question is also assessed. The parameters which are subject of the study are chosen to be such parameters which are needed in order to use the methods of 3D modeling and computer simulations in combination with the Finite element method and elasticity theory to perform analysis on the stress and deformational state of machine parts made of rubber. Conducting such analysis would allow the engineers to examine the influence of various factors related to the design of the machines on the distribution of stress within the rubber parts. This could be in favor of improving the design of the technological equipment and increase the life-span of the rubber parts.*

Key Words: NBR-based rubber compound, experimental study, mechanical properties, application in 3D FEM-based modeling

I. Introduction

Rubber is widely used material within the technological equipment used in the food processing industry. One of the most common application of the elastomers is related to the production of various gaskets intended to ensure proper insulation of environments filled with different fluids and/or operating at different pressure. It is crucial to prevent leakages and accidental mixing of fluids in the food processing equipment as one such leakage can cause a contamination of the food products and endanger the health of the consumers.

Efficient and reliable insulation is achieved by subjecting the rubber gaskets to a mechanical compressive loadings causing it to sustain deformation which is predominantly elastic. As the time passes however, ageing process of the rubber leads to irreversible change in the mechanical properties resulting in a residual plastic deformation and loss of functionality of the gasket which would require its replacement. Ageing can be accelerated either by aggressive chemical compounds are in direct contact with the gaskets or by subjecting the gasket to higher temperatures.

For the past two decades many elements related to the design of the technological equipment used in the food processing industry have been optimized and their functional characteristics have been improved. This optimization has been achieved by implementing advanced tools for enginery design such as CAD/CAM software products which by using the Finite element method (FEM) can determine and then visualize the distribution of the stress and deformation within 3D geometric models of various elements of the machines and apparatus used in the food processing industry.

Such advanced tools can be use to obtain information on the stress state within the gaskets and other rubber parts. This information can be used to assess the influence of different factors related to the design of the equipment and/or the rubber parts themselves. An optimization can be done aiming to prolong the life-span of the rubber parts and improve their reliability and functionality.

Knowledge of certain mechanical characteristics comes necessary in order to be able to use the means of 3D modeling combined with FEM and elasticity theory for obtaining of an accurate and useable picture of the distribution of the stress and deformation within the rubber parts inserted into the food-treating machines. Not only are some mechanical properties of rubber needed to be known, but how the ageing process of rubber affects them also comes essential.

The present article presents a study which has been conducted to determine some mechanical properties of NBR-based vulcanized rubber mixture which is most commonly used as material for O-shaped ring gaskets which are widely used in food-processing industry. The study also assesses the change of the determined mechanical properties due to the process of ageing of rubber.

The mechanical properties which are a matter of interest for the study are the modulus of elasticity E (also known as Young's modulus), tensile strength R_M and the rupture elongation A – properties needed for a numerical determination of the stress state of 3D geometric model by using FEM combined with

the elasticity theory. Shore A hardness is also examined.

II. Materials and methods

For the purpose of the study a NBR-based rubber mixture which is widely used for the production of O-shaped ring gaskets is chosen. The optimal vulcanization parameters (temperature and time) are determined by reading the vulcanization curve obtained by performing standard Mooney viscosity measuring on the mixture at temperature of 170° C.

A laboratory hydraulic machine (figure 2) is then used to form and vulcanize a rubber sheet from which tensile specimens are cut out. The tensile specimen and its dimensions are shown on figure 1. The thickness of each specimen is measured just before the test is conducted.

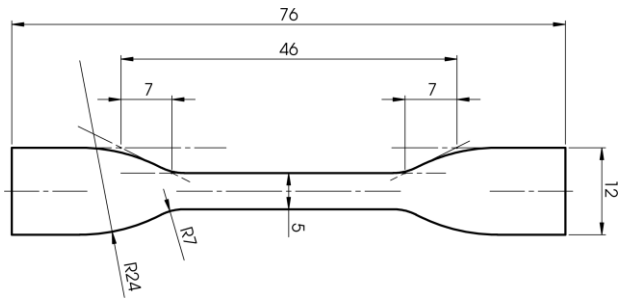

Figure 1. *Tensile specimen*

Additionally to measure Shore A hardness, disc-shaped specimens are formed and vulcanized – they are 30 mm in diameter and 12 mm thick.

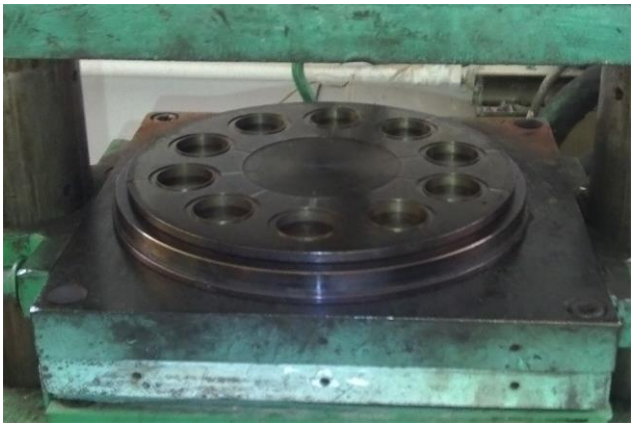

Figure 2. *Laboratory hydraulic machine for forming and vulcanizing of rubber specimens*

All the specimens are then separated into 4 groups. The samples from the first group are tested without being subjected to ageing while the other 3 groups are placed inside a specially designed heated chamber and are subjected to higher temperature (100°C) to accelerate ageing process. One of the group is tested after 24 h of ageing, the next group is tested after 48 h of ageing and the last group after 72 h of ageing.

From the tensile test of the specimens the "stress-strain" curve is obtained which is then used to determine the tensile strength, elongation and the modulus of elasticity. Measuring of Shore A hardness is done by using the disc-shaped sample.

Additionally, the residual deformation test is also conducted. The specimens used are the same disc-shaped samples which are used to measure Shore A hardness. They are placed between two steel circular plates (called "external plates") and pressure is applied by enclosing the plates until the deformation in the rubber disc, measured in the direction of the thickness of the sample, becomes equal to 25% percent. In order to ensure that the deformation will be 25%, a small steel ring is used (called "internal plate") whose thickness is chosen so it can fix the position of the external plates and the gab between them is always equal to the height of the deformed rubber specimen which is subjected to compressive loading between the external plates (see figure 3). After the external plates are "closed" with the rubber specimen between them, they are secured by using clamps and they are then placed into the heated chamber for a certain period of time at 100°C temperature so ageing process occurs. Then it is removed from the heated chamber, the plates are "opened" and the new thickness of the rubber disc is measured and compared to the original value of 12 mm and the relative residual deformation is determined in percentage. In total 3 samples are tested – one is aged in the heated chamber for 24 h, the second for 48 h and the third is aged in the heated chamber for the period of 72 hours.

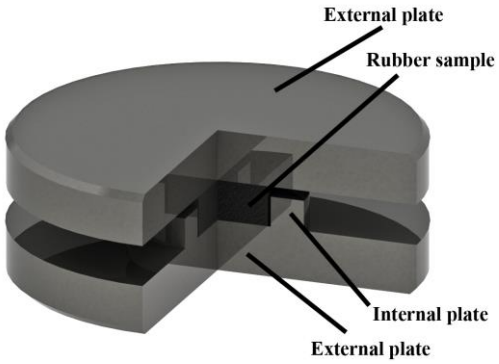

Figure 3. *Residual deformation test*

III. Results and discussion

The resulting vulcanization curve obtained after Mooney viscosity measuring is shown on figure 4.

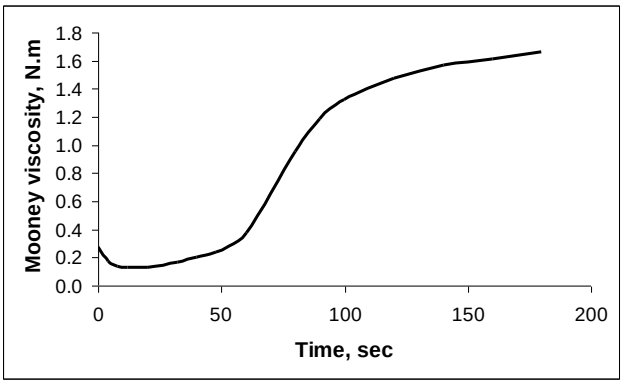

Figure 4. *Vulcanization curve*

The obtained "stress-strain" curves from the tensile tests of the specimens from the different groups are shown on figure 5. The curves shown on the figure are drawn from the average results from all specimens within each group. Tensile rate used is 500 mm/min. The air temperature during the experiments is 20 ±1 °C.

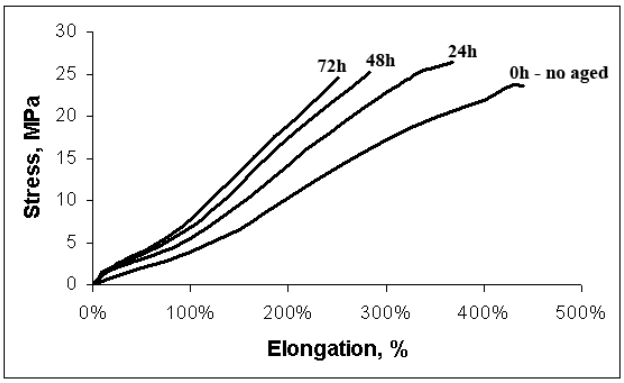

Figure 5. *"Stress-strain" curves*

The chart on figure 6 shows the registered change of the modulus of elasticity as result of the ageing.

Figure 6. *Change of the modulus of elasticity*

Figure 7 shows a chart which depicts the change of the tensile strength as an effect from the ageing process.

Figure 7. *Change of the tensile strength*

The change of the elongation is shown on figure 8 while the effects of the ageing over the Shore A hardness is shown on figure 9.

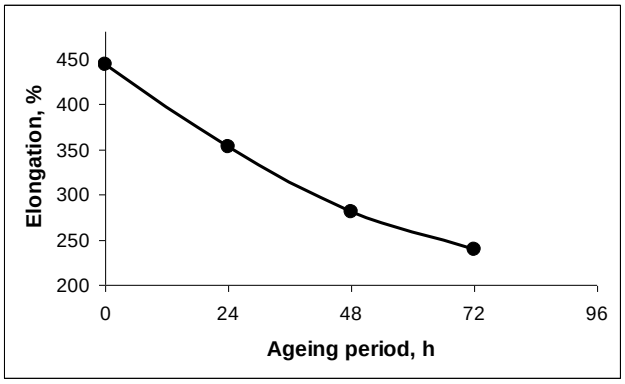

Figure 8. *Change of the elongation*

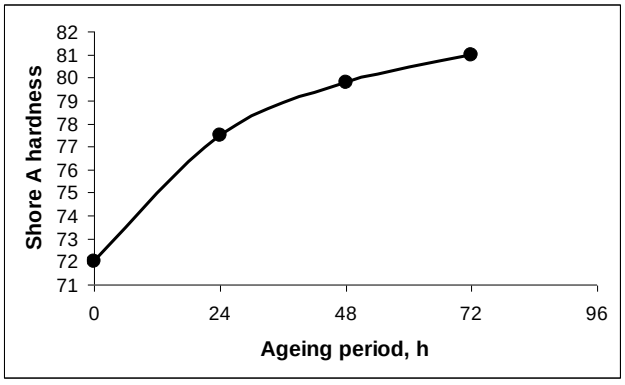

Firgure 9. *Change of the Shore A hardness*

The results clearly indicate that the ageing hardens the rubber – there is a rise in the modulus of elasticity and drop in the elongation. Shore A hardness is rising.

The tensile strength has risen after 24 h of ageing but it decreases if the ageing process is longer. This is explained with the fact that even after vulcanization takes place, there is still a potential to form more cross-linking chains within the elastomer. Then, further ageing process causes the cross-linking chains to break resulting in drop of the tensile strength of the rubber.

Since the modulus of elasticity is a matter of greater interest, which is because this property is crucial for conducting numerical studies by using the 3D modeling along with FEM and elasticity theory, the results related to the change of the modulus of elasticity shall be also represented with a mathematical equation.

Linear regressional equation is written as follows:

$$E(H) = 0{,}0636.H+6{,}9115$$

where:

- E – modulus of elasticity,
- H – ageing period.

The coefficient of determination R^2 for this equation is determined to be 0,95. The equation shows that by every 1 hour of exposure of the rubber at 100°C the occurring ageing process results in approximately 63,6 kPa rise in the modulus of elasticity of the NBR-based vulcanized rubber mixture.

The ageing of rubber in natural operational conditions shall also result in similar change of the mechanical properties, however it will happen in much slower rate [2], since the constant exposure at 100°C (as it is done during the experimental testings) results in accelerated ageing.

The residual deformation tests show that after being subjected to accelerated ageing while being compressed between two plates (figure 3), the rubber samples all have 7,3% residual relative deformation (the difference is very small). The consistency of this value, despite the different ageing periods, can be explained with the fact that there are still possibility left to form more cross-linking chains between the macromolecules of the elastomer – the rubber can still sustain some amounts of plastic deformation. When heated, additional cross-linking process is initiated and few more cross-linking chains are formed while the rubber is in a state of being subjected under compressive loading and is being deformed. This way, the rubber body undergoes a secondary forming and it simply takes a new shape.

IV. Conclusions

Experimental study has been conducted on specimens made of NBR-based vulcanized rubber mixture to determine some of its mechanical characteristics which would allow numerical studies to be made on the stress and deformational state of 3D models of rubber parts within machines and apparatus in food processing industry.

Data have been obtained about the change of the studied mechanical properties because of the ageing process of the rubber. The knowledge on this change would allow the ageing process to be taken into consideration when performing numerical studies on rubber parts by the means of 3D modeling in combination with FEM and elasticity theory.

Experiments have been conducted to determine the residual deformation of a NBR-based vulcanized rubber mixture as a result of compressive loading combined with the effects of ageing process of the rubber. This data could also serve in favor of building rather accurate and more reliable models of rubber parts in the machines and apparatus in the food processing industry.

References

1. Dong C.L., Yuan C.Q., Bai X.Q., Yan X.P., Peng Z., Tribologicalpropertiesofagednitrilebutadienerubberunder dryslidingconditions, Wear, p. 226-237, (2015), ISSN 0043-1648.
2. La Count B.J., Castro J.M., Hoover-Ignatz F., Development of a service-simulating, accelerated aging test method for exterior tire rubber compounds II. Design and development of an accelerated outdoor aging simulator, Polymer Degradation and Stability, 75 (2002), p. 213–227, ISSN 0141-391.

ISSN 1314-7773

Journal of **FOOD** and **PACKAGING** Science, Technique and Technologies

National Academy of Packaging-Bulgaria